Available online at www.sciencedirect.com
ScienceDirect
Journal of Sound and Vibration 322 (2009) 98–134
JOURNAL OF SOUND AND VIBRATION
www.elsevier.com/locate/jsvi

An FRF bounding method for randomly uncertain structures with or without coupling to an acoustic cavity

L.W. Dunne[a], J.F. Dunne[b,*]

[a]*Special Applications Department, CDH AG, Am Marktplatz 6, D-79336 Herbolzheim, Germany*
[b]*Department of Engineering and Design, School of Science and Technology, The University of Sussex, Falmer, Brighton BN1 9QT, UK*

Received 5 March 2007; received in revised form 8 May 2008; accepted 27 October 2008
Handling Editor: C.L. Morfey
Available online 7 January 2009

Abstract

An efficient frequency response function (FRF) bounding method is proposed using asymptotic extreme-value theory. The method exploits a small random sample of realised FRFs obtained from nominally identical structures to predict corresponding FRF bounds for a substantially larger batch. This is useful for predicting forced-vibration levels in automotive vehicle bodies when parameters are assumed to vary statistically. Small samples are assumed to come either from Monte Carlo simulation using a vibration model, or via measurements from real structures. The basis of the method is to undertake a hypothesis test and if justified, repeatedly fit inverted Type I asymptotic threshold exceedance models at discrete frequencies, for which the models are not locked to a block size (as in classical extreme-value models). The chosen FRF 'bound' is predicted from the inverse model in the form of the 'm-observational return level', namely the level that will be exceeded on average once in every m structures realised.

The method is tested on simulated linear structures, initially to establish its scope and limitations. Initial testing is performed on a sdof system followed by small and medium-sized uncoupled mdof grillages. Testing then continues to: (i) a random acoustically coupled grillage structure; and (ii) a partially random industrial-scale box structure which exhibits similar dynamic characteristics to a small vehicle structure and is analysed in NASTRAN. In both cases, structural and acoustic responses to a single deterministic load are examined. The paper shows that the method is not suitable for very small uncoupled systems but rapidly becomes very appropriate for both uncoupled and coupled mdof structures.

1. Introduction

Uncertainty complicates the design of dynamically sensitive structures in many areas of engineering including the automotive, aerospace, civil construction, and marine industries. Automotive vehicle-body design for example, is a compromise between competing factors, aimed mainly at minimising body-weight for better fuel economy. Lightweight vehicle structures are unfortunately prone to vibration and interior noise problems which unresolved, can adversely affect customer acceptance and driver safety. The analysis of noise, vibration, and harshness (NVH) forms an important part of vehicle design and refinement. A particular

*Corresponding author.
E-mail address: j.f.dunne@sussex.ac.uk (J.F. Dunne).

0022-460X/$ - see front matter © 2008 Elsevier Ltd. All rights reserved.
doi:10.1016/j.jsv.2008.10.035

problem is how to predict the NVH characteristics of production vehicles, since normal manufacture introduces variability into vehicle geometry, material properties, and suspension components. As a result, nominally identical vehicles can leave the assembly-line with widely different NVH characteristics (a number of which are not acceptable). The task facing the NVH analyst is how to envelope acoustic frequency response functions (FRFs) for an ensemble of production vehicles across the entire frequency range.

Three qualitatively different frequency regions can be identified for vehicle NVH analysis: the low, medium, and high frequency regions. At low frequency, the vibro-acoustic response exhibits marked modal behaviour, whereas in the mid-frequency range (where wave-lengths are shorter) FRFs are very sensitive to material properties and detailed boundary conditions. At high frequency (where modal density and overlap are high) the ensemble average frequency response becomes smooth, and depends less on detailed boundary conditions. In the early stages of vehicle structural design, computer-based dynamic analysis is undertaken using detailed finite element (FE) models to obtain low frequency vibration characteristics. To predict passenger-space acoustic noise levels, an FE model of the air-interior volume is coupled to an FE structural model. But owing to variability in the actual physical structure, many model parameters are uncertain and cannot be treated as deterministic variables. Deterministic analysis therefore provides no information about the statistical nature of low frequency responses. A formal non-deterministic approach involves direct randomisation of the equations of motion [1–3]. Indeed in the mid-frequency region, methods have been proposed to combine deterministic and statistical techniques for predicting steady-state ensemble-average responses of complex vibro-acoustic systems [4]. At high frequency, statistical energy analysis (SEA) can be used [5–7], where the time-averaged vibration power transfer between individual sub-systems can be related to equilibrium energies. These methods are, however, not suitable in the low frequency region for non-deterministic analysis of structures with many degrees-of-freedom (dof).

Various methods which include uncertainty within structural analysis, are in principle suitable for low frequency dynamic response prediction. Parametric uncertainty for example can be modelled either as probabilistic or possibilistic [8]. Probabilistic uncertainty is described by a joint probability density function for the parameters, whereas possibilistic uncertainty uses a set of bounds on possible values. Many probabilistic methods exist within structural reliability theory [9] to compute failure probabilities. This mainly involves computation of multi-dimensional integrals. Monte Carlo simulation offers one of the most direct routes [10,11], but for large industrial-scale problems, the size of the corresponding FE models needed, renders these computations prohibitively expensive, making efficient alternatives absolutely essential. The first- and second-order reliability methods of FORM and SORM [12–14], potentially offer an efficient alternative, although these methods are complicated for a realistic number of uncertain parameters (since a constrained minimisation problem must be solved). By contrast, the stochastic FE method [15,16] offers no significant improvements in efficiency, whereas approximate alternatives, such as the (computationally efficient) response moment method [9,13], can suffer from serious inaccuracy.

Possibilistic methods by contrast, give worst-case predictions, and are more appropriate when statistical parameter information is unavailable. These include: 'interval analysis' [17–19], convex methods [20], and fuzzy modelling [21,22]. Accurate bounds on parameter variability is generally needed, and in practice, these methods also reduce to a large-scale minimisation task.

Various methods have focused specifically on bounding FRFs [23]. For small problems, bounds can be calculated using the so called 'vertex method', or more generally, by solving an optimisation problem. Elsewhere a numerical scheme is introduced in [24] to envelope the FRF of a damped FE model with fuzzy uncertain parameters. This leads to the 'modal rectangle (MR) method', which is further improved (by coupling modal stiffness and modal mass) in the 'modal-rectangle-method-with-eigenvalue-interval-correction-method' (MRE). A fuzzy FE procedure for FRF bounding has also been applied in [25], where four case-studies on small structural models demonstrate that inherent conservatism in the MR method is reduced by the MRE method. In yet a different approach, so called 'affine' analysis was proposed in [26], recognising that interval analysis generally overestimates an FRF because it cannot account for dependency between modal variables. Test examples using small structures, demonstrate that affine-based FRF bounds are lower than those obtained by complex interval analysis. Fuzzy intervals were also used in [22] to account for parameter uncertainty in the 'transformation method' (TM) [21], which is applicable if the output is monotonic, where interval arithmetic is replaced by a set of deterministic computations. The TM is

accurate but computationally very expensive, and to overcome this drawback, the 'short transformation method' (STM) was proposed in [22] as an efficient alternative. A component mode (CM) TM (which also falls within a fuzzy framework) is described in [27] where emphasis is placed on the computational efficiency of the CM compared to alternatives.

An approximate numerical approach for bounding FRFs is described in [28] using an FE model with uncertain parameters in the mass and stiffness matrices. Conservative approximations are used to find single mode FRF envelopes which combine to produce the total FRF envelope. Different modal space formulations and approximations are examined, in particular, the standard specific modal mass and stiffness approach, plus use of a modal constant and eigenvalue. The MR is compared with (the preferred) MRE method by testing on a four mass–spring system using eight uncertain interval variables and diagonal damping. A 'vertex identification method' (VIM) is proposed in [29] to identify the parameter combination that yields the maximum FRFs. Interval bounds are considered to exist on the mass and stiffness parameters. For these frequency ranges excluding a resonance, a quasi-convex FRF property is exploited. This guarantees that the maximum FRF occurs on one of the vertices of a hypercube defined by the interval parameters, leading to an approximate approach which is exact when the FRF is monotonic. Direct use of the vertex method requires $2^{(N_M+N_K)}$ sets of calculations, whereas the more efficient VIM only requires $2(N_M+N_K)$ evaluations. The VIM is improved with a near-resonance correction, yielding excellent FRF bounds over the complete frequency range when tested to obtain point receptances for a lumped-mass structure (with a few dof).

The dynamic response of vehicle structures (coupled to an acoustic cavity) generally involves many thousands (or even millions) of dof and a very substantial number of uncertain parameters. It is clear from the literature that no suitable probabilistic method is yet available for bounding low-frequency FRFs of large systems. Asymptotic extreme value (EV) theory by contrast is now well developed [30], but this has never been used specifically to predict the behaviour of uncertain structures. And yet, it is possible to hypothesise that high FRF values associated with an ensemble of uncertain structures fall into the category of EVs. For general application, such a hypothesis requires careful examination to first reconcile any obvious physical limitations, and second to establish where it holds good in terms of model size, frequency range, and types of uncertainty. This examination needs to address uncoupled structures initially and then move on to structures coupled to an acoustic cavity.

In this paper, asymptotic EV theory is exploited to develop a statistical method for predicting 'practical' bounds on the FRFs associated with a specified number of uncertain structures but using a significantly smaller set of FRF realisations. The objective is ultimately to establish whether this method can be used for moderate and industrial-scale structures coupled to an acoustic cavity, assuming FRF samples can be generated via a model and Monte Carlo simulations.

2. An FRF bounding method via asymptotic EV theory

The problem of FRF bounding for stable linear structures will now be made specific, starting with the description of a linear dynamic model of an uncertain structure. This model will ultimately be used in Monte Carlo simulation to generate data of various sample sizes needed to test the proposed prediction method developed. This development takes place after three things have been outlined. First the classical asymptotic GEV model is discussed even though it is actually not used for FRF bounding. This is discussed to allow the second topic, namely the threshold-exceedance model, to be put into context, its benefits highlighted, and different interpretations of *quantile* predictions based on *return levels* to be reconciled. Third, the so called Hasofer–Wang hypothesis test is described which is used prior to prediction, to decide whether use of the proposed method is justified. In the final part of the section, the proposed prediction method is summarised.

The equations of motion of a stable linear structure driven harmonically by excitation vector $\mathbf{P}(t)=\mathbf{P}e^{i\omega t}$ can be written in the form:

$$(-\omega^2[\mathbf{M}]+i\omega[\mathbf{C}]+[\mathbf{K}])\mathbf{Y}=\mathbf{P} \tag{1}$$

for which the displacement response is $\mathbf{Y}(t)=\mathbf{Y}e^{i\omega t}$, and where ω is the excitation frequency. The mass, damping, and stiffness matrices depend on unknown variables denoted by parameter vector $\mathbf{X}$, and can be written in the form $\mathbf{M}(\mathbf{X})$, $\mathbf{C}(\mathbf{X})$, and $\mathbf{K}(\mathbf{X})$, which in general, are also frequency dependent. For prescribed

vector **X**, Eq. (1) can be solved exactly to yield the response **Y**, which in general includes the acoustic response for a structure coupled to an air cavity. The approach adopted to handle probabilistically uncertain structures, is to model each unknown variable with a probability density function $p(\mathbf{X})$—the aim being to derive particular statistics associated with the response. At any given frequency ω, this probabilistic description relates directly to a particular FRF of interest, which allows the statistics of the FRF to be computed such as the mean and standard deviation. However, with increasing problem size, the search for an absolute bound on the FRF (the existence of which may be justified by physical argument) becomes increasingly difficult if one remains within a probabilistic framework. Conversely, knowledge of an explicit FRF bound may be of little practical value when uncertain parameters do indeed vary statistically. The problem then for a realistically large structure, is that the likelihood of a bound being reached is simply too remote to be of practical consequence. A much more useful measure is a statistic that focuses on very rare high-level responses.

The particular problem for FRF bounding is therefore considered as follows: for some arbitrary frequency ω, with interest focused on one particular type of FRF $H(j\omega)$, the generation of N realisations of parameter vector **X** would lead to N realisations of **M**(**X**), **C**(**X**), and **K**(**X**), and a vector of (realised) complex FRFs $\mathbf{H}=\{H_1(j\omega)\ H_2(j\omega)\dots H_N(j\omega)\}$. The particular task is to estimate from some small sample of size N_s, the absolute maximum modulus value of all the realisations in **H** corresponding to some hypothetically large value of N. The small sample size N_s corresponds for example, to a value that could in practice be achieved using Monte Carlo simulation with a large-scale FE model. The difficulty, for realistically large structures with many uncertain parameters, is that even if the existence of a bound can be accepted on physical grounds the number N would, in practice, have to be extremely large for the maximum response to even approach the bound. In other words, the probability of realising the particular structure that would put the FRF on the bound, would be practically zero. This is an obvious philosophical limitation with attempting to compute the probability associated with a physical FRF bound for a structure with probabilistically varying parameters. The description of a 'practical' (probabilistic) bound does, however, fall neatly within the theory of EVs. An approach is now developed which makes use of an asymptotic threshold exceedance model, where it will be assumed that the predicted level (or quantile), associated with a specified FRF EV probability, provides a 'practical' bound. Such practical bounds are wholly consistent with a probabilistic model for uncertainty and are intended for use with small amounts of data (generated perhaps using a detailed FE model or measured from real structures). The key step is to treat the vector of modulus values of the components in **H** as forming a set of independent identically distributed random variables—precisely the requirement for which EV theory has been developed. To outline the EV theory, the classical asymptotic EV model is initially explained to show why it is actually not suitable for FRF bounding. This is in contrast to an alternative description of extreme events, namely the asymptotic threshold exceedance model which is shown shortly to be very suitable under appropriate circumstances.

2.1. Classical asymptotic EV theory

Classical EV theory [30,31] focuses on the statistical properties of variable $M_n=\max\{X_1,X_2,\dots,X_n\}$, where X_i is a sequence of independent, identically distributed random variables. An important aspect of extreme-value analysis is the prediction, with specified exceedance probability p, of the level or *quantile* $z(p)$ that will be exceeded by random variable M_n i.e. $Pr\{M_n>q(z)\}=p$. To derive an asymptotic family of EV distribution functions, the theory proceeds by normalising variable M_n using a sequence of 'scale' and 'location' parameters $\{a_n>0\}$, and $\{b_n\}$, such that:

$$M_n^*=\frac{M_n-b_n}{a_n} \tag{2}$$

An important extreme-value theorem [30, p. 46] shows that when M_n can be stabilised, the limiting distribution $G(z)$ i.e.:

$$Pr\left\{\frac{M_n-b_n}{a_n}\leqslant z\right\}\to G(z)\quad \text{as}\ n\to\infty \tag{3}$$

belongs to one of three asymptotic types: Type I being a Gumbel, Type II a Fréchet, and Type III a Weibull distribution. These distribution functions can be expressed explicitly in three separate forms, or as a single three-parameter generalised extreme-value (GEV) distribution:

$$G(z) = \exp\left\{-\left[1+\xi\left(\frac{z-\mu}{\sigma}\right)\right]^{-1/\xi}\right\}, \quad 1+\xi\left(\frac{z-\mu}{\sigma}\right)>0 \tag{4}$$

where the scale σ, location μ, and shape ξ parameters, respectively, satisfy inequalities $\sigma>0$, $-\infty<\mu<\infty$, and $-\infty<\xi<\infty$. It can be shown [30] that the case $\xi>0$ corresponds to a Type II distribution which models an EV bounded from below, the case $\xi<0$ corresponds to a Type III which is bounded from above, and the case $\xi=0$ corresponds to a Type I distribution which is completely unbounded and can be written in the form:

$$G(z) = \exp\left[-\exp\left\{-\left(\frac{z-\mu}{\sigma}\right)\right\}\right], \quad -\infty<z<\infty \tag{5}$$

In practice, when working with finite data sample sizes n, it is assumed that the extreme data is closely approximated by a GEV Eq. (4) such that:

$$Pr\left\{\frac{M_n-b_n}{a_n}\leqslant z\right\} \approx G(z) \tag{6}$$

Measured data is usually used to determine which asymptotic model is appropriate. But because Eq. (6) is strictly only an acceptable model when the data is extreme, some pre-processing is often necessarily. Three approaches that are used for pre-processing data: one route is to sub-divide sections into data 'blocks' [30], a second approach uses a specified high-level data threshold [30], and a third route involves selecting top-order statistics [32]. For time series, putting data into 'blocks' is a natural procedure for estimating the parameters in a classical EV distribution, where the block-size corresponds to a specified duration. For an arbitrary vector of size N_{Total}, however, blocking is strictly the only correct procedure for fitting a GEV. This involves sub-sectioning a vector of raw data into N_B 'blocks', and then taking only one maximum value from each block. These maximum values (obtained from a number of blocks) are then used for parameter estimation. The fitted parameter values in the GEV are then locked to N_{Pb}, the number of data points in each block where $N_{\text{Total}} = N_{\text{Pb}} \times N_B$. Blocking in this way can, however, be a wasteful process because useful data is sometimes excluded. For example because only one maximum is collected per block, it is possible that the next highest value in a block is actually greater than the maximum in a different block. To circumvent this problem, the two alternative approaches are used to find a compromise between bias and variance by attempting to sample more useful extreme data. The selection of a data threshold is a device to sample only high level data which exceeds the threshold so that more good data will be selected than via blocking. The main difficulty is to decide on the threshold. By contrast, the use of 'top-order statistics' where the entire raw data vector is ranked into ascending order and only the top k values are used for estimation also has the capability of sampling more good data than blocking. But here the difficulty is to have some basis for selecting the top-order value k. Various semi-empirical approaches have been developed to provide a basis for selecting both the threshold level, and the top-order value k.

A calibrated GEV can be used to predict quantiles. A particularly useful measure is the *return level* z_p associated with a *return period* $1/p$, which, for blocked EVs, is the inverse solution of $Pr\{M_n>z(p)\}=p$ obtained in algebraic form by inverting Eq. (4) where the exceedance probability is $p=1-G(z_p)$. The *return level* associated with a GEV model, can be interpreted (to a very good approximation) as that threshold which in $N_B=1/p$ blocks would on average be exceeded just once. Since the parameters in a GEV are locked to the number of data points per block N_{Pb}, the *return level* z_p is only suitable for extrapolating to exceedance levels for integer multiples of $N_B \geqslant 1$. It cannot be used to extrapolate to different values of N_{Pb} which is a requirement for FRF bounding. Moreover this limitation is compounded for a GEV model when data pre-processing uses either a threshold or top-order statistics approach. Fortunately the problem can be avoided by not using a GEV at all but rather by using an asymptotic threshold exceedance model as now explained.

2.2. The asymptotic threshold exceedance model and the m-observational return level

The asymptotic threshold exceedance model [30] is analogous to the GEV and can in fact be related to it. A practical advantage of using an asymptotic threshold exceedance model is that it is possible to make extreme level quantile estimates via a *return level* similar to a GEV model but relating to a fractional multiple of the data in a block, without the model depending on the block sample size N_{Pb}. Furthermore the process of fitting the model can be much simplified because the selection of the required data threshold is achieved in terms of 'top-order statistics' [33] for which a very simple semi-empirical criterion is available to select the top-order value k.

The asymptotic threshold exceedance model is defined in terms of a conditional exceedance probability associated with an independent and identically distributed sequence of random variables. In particular, by denoting an arbitrary term in the sequence as X, the model can be defined as the exceedance probability conditional on a realisation having already exceeded some high threshold u, namely:

$$Pr\{X>u+y|X>u\}=\frac{1-F(u+y)}{1-F(u)},\quad y>0 \tag{7}$$

For large u, it can be shown (in the form of a theorem [30, p. 74]) that $Pr\{X<u+y|X>u\}$ can be approximated (in asymptotic form) as a three-parameter generalised Pareto distribution:

$$H(y)=1-\left(1+\frac{\xi y}{\bar{\sigma}}\right)^{-1/\xi} \tag{8}$$

where $y=X-u>0$, $1+(\xi y/\bar{\sigma})>0$, and $\bar{\sigma}=\sigma+\xi(u-\mu)$. The theorem which leads to Eq. (8) shows that if there exists a GEV (i.e. for 'blocked' maxima), then there is a corresponding asymptotic model for high threshold exceedances of u within the generalised Pareto family. Indeed analogous to a GEV, when parameter $\xi<0$, the Pareto distribution has an upper bound $u-\bar{\sigma}/\xi$, whereas for $\xi>0$, the distribution has no upper bound. For the special case $\xi=0$, the generalised Pareto family reduces to a limiting case exponential distribution with parameter $1/\bar{\sigma}$, namely:

$$H(y)=1-\exp\left(-\frac{y}{\bar{\sigma}}\right) \tag{9}$$

An exceedance probability estimate associated with variable X, based on n realised samples of data, can be obtained using Eq. (7) and the generalised Pareto distribution Eq. (8), in the form:

$$Pr\{X>x|X>u\}=\frac{Pr\{X>x\cap X>u\}}{Pr\{X>u\}}=\left[1+\xi\left(\frac{x-u}{\sigma}\right)\right]^{-1/\xi} \tag{10}$$

where the scale parameter $\bar{\sigma}$, specific to the generalised Pareto distribution in Eq. (8), can from now on be denoted simply by parameter σ. By re-arranging Eq. (10), and noting that $Pr\{X>x\cap X>u\}=Pr\{X>x\}$, the exceedance probability can be expressed as

$$Pr\{X>x\}=Pr\{X>u\}Pr\{X>x|X>u\}\approx\frac{k}{n}\left[1+\xi\left(\frac{x-u}{\sigma}\right)\right]^{-1/\xi} \tag{11}$$

where $Pr\{X>u\}\approx k/n$; k is the number of realisations above threshold level u, within the total number of realisations n.

Quantile estimation can be made via Eq. (11) in terms of the m-observational return level x_m. This is defined as the level that will be exceeded by variable X on average once every m observations (of data). By equating the exceedance probability as $Pr\{X>x\}=1/m$, Eq. (11) can be inverted to give a quantile estimate in terms of the m-observational return level:

$$x_m\approx\frac{\sigma}{\xi}\left(\left(\frac{n}{mk}\right)^{-\xi}-1\right)+u \tag{12}$$

For a Type I model, namely when $\xi = 0$, the return level estimate via Eq. (9) takes the form:

$$x_m \approx \sigma \log\left(\frac{mk}{n}\right) + u \tag{13}$$

Before discussing the threshold exceedance model fitting process, a very important distinction can be made between the Type I m-observational return level x_m from Eq. (13), and the Type I *return level* z_p associated with a GEV discussed in Section 2.1. It can be shown that for a Type I model [30], the threshold exceedance model parameter σ in Eq. (9), is completely independent of the threshold level u. Moreover, for a Type I model, if the threshold level (parameter) u is correctly selected then the model can be used to make predictions for arbitrary values of m. This is in stark contrast to the *return level* z_p which depends implicitly on N_{Pb} the amount of data in a block. The question then for a Type I model, is how should the threshold exceedance model parameters σ and u be estimated.

2.3. Threshold exceedance model parameter estimation using 'top-order statistics'

Selection of threshold u should be made as low as possible to capture sufficient data, but should not be too low otherwise the asymptotic model assumptions will be violated. In general, very accurate selection is difficult (for example via the 'mean residual life plot' [30, p. 78]) where the main problem is one of interpretation. Alternatively, and indeed the procedure adopted here, is to exploit the use of top-order statistics [33] to fit Eq. (13). An unbiased maximum likelihood estimate of σ can indeed be achieved via top-order statistics whereas selection of u is based on the assignment of a particular value of data based on the value of the top-order statistic k. A semi-empirical basis is used to select k and therefore to select u. From a practical viewpoint this is attractive but its inherent empiricism may lead to bias in predictions that may justify correction based on experience. Returning to the general parameter estimation problem associated with Eq. (8), when the threshold level u remains implicit, the parameters of the generalised Pareto distribution can be obtained using maximum likelihood estimation. The general form of log-likelihood function derived from Eq. (8) is

$$l(\sigma, \xi) = -k \log \sigma - \left(1 + \frac{1}{\xi}\right) \sum_{i=1}^{k} \log\left(1 + \frac{\xi y_i}{\sigma}\right) \tag{14}$$

and for a Type I model when $\xi = 0$, the log-likelihood function takes the form:

$$l(\sigma) = -k \log \sigma - \sigma^{-1} \sum_{i=1}^{k} y_i \tag{15}$$

Explicit maximisation of the log-likelihood function is not generally possible, but for Type I an estimate for σ is given as

$$\sigma = \frac{\sum_{i=1}^{k} y_i}{k} \tag{16}$$

which in terms of the m-observational return level x_m gives the quantile estimate using Eq. (13) as

$$x_m \approx \frac{\sum_{i=1}^{k} y_i}{k} \log\left(\frac{mk}{n}\right) + u \tag{17}$$

Now by rewriting the summation in Eq. (16) as

$$\sum_{i=1}^{k} y_i = \sum_{i=1}^{k} x_i - ku \tag{18}$$

the parameter estimate via Eq. (16) then becomes:

$$\sigma = \frac{\sum_{i=1}^{k} x_i}{k} - u \tag{19}$$

and by setting $\sigma = \hat{a}$ in Eq. (16), and $u = x_{kn}$ (where x_{kn} is the 'kth descending top-order statistic' [33] for sample size n), and by setting $\hat{x}_m = \hat{q}(m)$, Eq. (17) can be written as

$$\hat{q}(m) \approx \hat{a} \log\left(\frac{mk}{n}\right) + x_{kn} \tag{20}$$

Therefore, when the data has been established to be Type I, Eq. (20) is the 'best-linear-unbiased-estimator' or so-called 'Weissman' estimator [32] based on k top-order statistics. The selection of the optimal top-order statistic k for use with the Weissman estimator, is in general difficult but a simple semi-empirical value expressed as a function of n is recommended in [32], namely:

$$k = 1.5\sqrt{n} \tag{21}$$

Approximate confidence intervals can also be constructed for Type I quantile estimates [32] using the standard deviation associated the estimator Eq. (20) i.e.:

$$\sigma(\hat{q}) = c_n\left[\varsigma_n^2 \frac{(k-1)}{k^2} + \frac{\pi^2}{6} - R_k\right] \tag{22}$$

where $\zeta_n = \log(km/n)$, $c_n = \hat{q}(ne) - \hat{q}(n)$, $R_k = \sum_{n=1}^{k-1} n^{-2}$ and $e = 2.718\ldots$ i.e. the natural number e. In summary then, when it can be established that the data is consistent with a Type I model, the use of the Weissman estimator (Eq. (20)) is attractive because: (i) it is simple, and avoids explicit parameter estimation, (ii) a recommended value for k (the top-order statistic) is available, and (iii) approximate bounds on the confidence of the predicted quantiles can be constructed. As stated earlier, the only reservation is that this approach to selection of threshold u may lead to bias and this should be accounted for when interpreting predictions. The remaining question then is how the type of data can be established. This is achieved via a dedicated hypothesis test as now explained.

2.4. Hasofer–Wang hypothesis test

It is important to establish the particular 'domain of attraction', namely Type I, II, or III to which the data belongs. This is because the statistical properties of the tail behaviour can be suitably modelled by an appropriate asymptotic distribution. This process essentially requires a test of hypothesis which is particularly relevant to the problem of bounding the frequency response of an uncertain structure. Even though pointed-out in [34], that there are good physical reasons why extremes of vibration data should actually be of Type I, a suitable test is needed before the Weissman type I estimator can be used with confidence. The Hasofer–Wang hypothesis test [30] provides a simple means of checking the domain of attraction using test statistic:

$$W = \frac{k(\bar{X} - X_{kn})^2}{(k-1)[\sum_{i=1}^{k}(\bar{X} - X_{kn})^2]} \tag{23}$$

where

$$\bar{X} = \frac{\sum_{j=1}^{k} X_j}{k} \tag{24}$$

This statistic is a function of k, the number of top-order statistics. For values of k around $1.5\sqrt{n}$ (as recommended in [30]) the following conditions are tested: Let W_U and W_L be the upper and lower percentage points for W (as supplied in Table 4.1 [32]), and let H_2 and H_3 denote the hypotheses that the extreme data, respectively, belongs to a Type II or III distribution. Then, if W is less than W_L, accept H_2: i.e. X belongs to the domain of attraction of Type II, while if W is greater than W_U, accept H_3: i.e. X belongs to the domain of attraction of Type III. Otherwise, it is accepted that X belongs to the domain of attraction of Type I allowing use of the Weissman Type I estimator.

2.5. A summary of probabilistic FRF bounding via the m-observational return level

We now return to the problem of FRF bounding as described at the beginning of the section and make appropriate use of the asymptotic EV theory discussed. To recall, the objective is to establish in a probabilistic sense, across the frequency range, an upper limit on the absolute values of the components in a chosen frequency response vector $\mathbf{H}$ which is realised as a consequence of variability in the nominal structure. It is assumed that only a small sample $n = N_s$ of such structures is realisable through model-based computations or through actual measurements on (or obtained from) real structures, and predicted bounds are to correspond to some larger number $N \gg N_s$. Typically the sample size N_s might be in the region of a hundred, possibly a few hundred whereas bounds may be needed for N structures in the thousands, or tens or even hundreds of thousands. The proposed bound chosen, is in fact the Type I quantile estimator or *m-observational return level* for asymptotic threshold exceedance model (of Section 2.2) corresponding to the value $m = N$. This is also known as the Weissman estimator (Eq. (20)), when use is made of the k top-order statistics to select the threshold level u (after Eq. (19)), and the maximum likelihood estimator Eq. (16) for model parameter σ. An empirical basis for choosing the top-order value k, justified in [33], is obtained by setting $n = N_s$ in Eq. (21). The particular merit of using a Type I threshold exceedance model for FRF bounding is that the parameter σ is totally independent of threshold u. Moreover the calibrated parameter σ and threshold u are not functions of $m = N$ but rather subject to statistical scatter depending on the magnitude of N_s. If N_s is small, then the level of confidence will be correspondingly lower but approximate confidence bounds on the quantile estimates can be constructed using Eq. (22).

In summary then, the probabilistic bound applying to a sample of N structures, based on the *m-observational return level*, is that level which will be exceeded on average once in a random sample of $N = m$ structures. To compute this bound the following steps are appropriate:

- Obtain a small sample $n = N_s \ll N$ FRFs at an appropriate set of discrete frequencies.
- Undertake a Hasofer–Wang hypothesis test at each frequency to establish the type of data. If the test indicates that the data is not of Type I, then predictions should not be attempted using the proposed method.
- If the data at discrete frequencies is of Type I, then Eq. (20) can be used to compute the bounds for a sample size of $m = N$ structures, putting approximate confidence bounds on the estimates via Eq. (22). If only an estimate of the *m-observational return level* is acceptable then that will be deemed as the bound, but if a more conservative bound is needed to account for statistical scatter then the level set by the upper confidence bound could be used.
- The predicted bound across the frequency range can be compared with the FRF for the nominal structure and compared with the maximum FRF values for the N_s sample structures realised.

3. The scope of EV-based structural FRF bounding

The proposed FRF bounding method will now be assessed to address its applicability, limitations, and computational efficiency to justify its use on relatively large linear systems coupled to an acoustic cavity in Sections 4 and 5. An interesting question is whether the method can be used to bound the frequency response of general uncertain nonlinear structures with arbitrary dof and including, for example, coupling through fluid–structure interaction or rotor-dynamic effects. While this is not addressed in detail here, it appears that there are no obvious reasons why the proposed approach could not be applied to bound stable FRFs from such structures where these can be adequately described and appropriate data is generated through Monte Carlo simulation. Two, more pertinent, questions concern the frequency range over which the method can be used for: (i) linear structures without any form of coupling and (ii) linear structures coupled to an acoustic cavity. Since the answer to the first question provides an important guide to the answer to the second, a systematic study is undertaken in the next section to assess the scope and limitations of the method. This starts with an uncertain sdof oscillator. The focus then moves to a small uncoupled mdof grillage structure with different types of uncertainty, and then on to an appropriately sized uncoupled grillage model which is designed to show up the capability of the method for uncoupled structures. The subsequent findings have

important implications for application of the method to structures coupled to an acoustic cavity. The final part of the section makes clear the computational advantages of the proposed method.

3.1. Applicability of the method

In assessing the applicability of the method to linear systems (not initially coupled to an acoustic cavity) different sources of uncertainty are important, in particular, the level of randomness in the mass and stiffness, and additionally, in the damping. In general, the type of mdof damping model determines whether the structure can be modelled as a modal system, which in turn, influences the frequency response of mdof systems. It would be expected that a modal system, in which there is low modal participation at resonant frequencies, would provide a particularly good mdof test of the proposed bounding method. Indeed if it can be established for an uncoupled system, that the method works well at resonant frequencies with low modal participation, then physical arguments can be used to assert that the method would work even better at acoustic peak frequencies when the structure is coupled to an acoustic cavity. This justification stems from the broad participation of structural modes to acoustic responses. Similarly it can be argued that if the bounding method works well on uncoupled structures at low frequencies, it should work better at frequencies away from resonance, and also at increasingly high frequencies. The focus in this section therefore remains on verifying the method for uncoupled structures at low frequency.

In attempting to justify general application of the method for uncoupled structures, two routes could be attempted: (i) theoretical verification or (ii) via an empirical route. Theoretical verification requires at each frequency, construction of the FRF distribution function $F(z)$ as a function of the distributions of the different sources of uncertainty in mass, damping, and stiffness. By either examining the properties of $F(z)$ in Eq. (7) as the threshold u is increased, or by examining the limit of $F^n(z)$ as $n \to \infty$, would in principle allow the EV type to be established, namely the type of Pareto distribution applying in Eq. (8) or the GEV type in Eq. (4). To be specific, computation of element (r,s) in the FRF matrix of an M dof system, can in general be expressed in the form [35]:

$$H_{rs}(\mathrm{i}\omega) = \sum_{j=1}^{2M} u_{rj}\left(\frac{1}{\mathrm{i}\omega - \lambda_j}\right)s_{js} \tag{25}$$

where λ_j are the system eigenvalues and u_{rj} are the upper elements of the $2M \times 2M$ modal matrix $[\mathbf{U}]$ associated with the model in state space, and where $s_{js} = \sum_{j=1}^{M} \upsilon_{jk} a_{ks} \upsilon_{jk}$ are the right-hand elements of $[\mathbf{U}]^{-1}$, and a_{ks} are the elements of the mass matrix $[\mathbf{M}]$. The corresponding absolute magnitudes of the FRF can be obtained using Eq. (25) in $|\omega^k H_{rs}(\mathrm{i}\omega)|$ taking $k = 0$, 1, or 2, respectively, for a receptance, mobility, or inertance function [35]. Unfortunately this theoretical route is unlikely to be successful for general mdof systems because the probabilistic distribution of the eigenvalues cannot in general be related explicitly to a probabilistic description of the system matrices, which in turn are nonlinear functions of the system geometry and material properties. Moreover, such verification is near impossible when measurements are obtained directly from real structures. The alternative, namely an empirical assessment, involves direct collection of response samples from a system model, a test of hypothesis, and if justified, quantile prediction in the form of the *m-observational return level*. In addition, verification by direct estimation of the *return level* is desired when appropriate. Empirical assessment obviously lacks the generality and insight that is produced by theoretical verification, but given the intractability of theory, an empirical approach based on Section 2 is justified here to assess the method for a sdof model, followed by small and medium-sized uncoupled grillage models.

3.1.1. Single-dof system

Empirical assessment of an uncertain sdof oscillator can actually be supported by the well-known FRF (receptance) version of Eq. (25) namely:

$$\left|H_y(\mathrm{i}\omega)\right| = \frac{1}{m}\left[\frac{\omega^2}{(\omega_n^2 - \omega^2)^2 + (2\zeta\omega\omega_n)^2}\right]^{1/2} \tag{26}$$

If the mass is kept constant, and only the stiffness is varied randomly, but the damping is varied in such a way to keep the damping factor ζ constant, then harmonic excitation at one frequency will produce a random steady-state response that will most definitely be bounded. For example the maximum possible amplitude that would be produced at the resonant frequency is $|H_y(i\omega_r)| = 1/m(2\zeta)$. For empirical verification, an oscillator has been chosen with fixed unit mass of magnitude $m = 1$, and fixed excitation frequency $\omega = 1\,\mathrm{rad/s}$. A randomly selected stiffness parameter is drawn from a uniform distribution with coefficient of variation (COV) = 0.2, such that the oscillator has varying natural frequency ω_n with a mean value = 1 rad/s. For each realised value of stiffness, the damping coefficient is selected to produce a constant damping factor $\zeta = 0.05$ (i.e. fixed at 5 percent critical). This means that each realisation of the oscillator will resonate near to the excitation frequency (indeed in most cases slightly above or slightly below it). The response amplitude is clearly bounded at the resonant amplitude $1/(2\zeta) = 10$, and therefore EVs would be expected to approach a Type III model.

The response of the oscillator with these parameter properties has been examined via Monte Carlo simulation. A total of 300 random samples of response amplitude are shown in Fig. 1a, both as realised, and in ascending order. Application of the Hasofer–Wang test of Section 2.4 is shown in Fig. 1b, using Eqs. (23) and (24) for various values of k top-statistics, showing 95 percent confidence bounds. Fig. 1a clearly shows that maximum values are indeed bounded, and in fact, the Hasofer–Wang test in Fig. 1b, gives strong support to the hypothesis that the data is Type III. In accordance with the summary of the proposed method in Section 2.5, FRF bounding should not be attempted because the data is not of Type I (and therefore does not enjoy the advantages discussed in Section 2.3 in respect of model parameter invariance and confidence bound construction). Despite this limitation, however, in this particular case a Type III extreme exceedance model Eq. (11) has been fitted to the data and inverted to obtain the corresponding quantile predictor. It is not the intention here to propose Type III models for general use in FRF bounding but rather to demonstrate that EV models do indeed give an indication of deterministic bounds. Fig. 1c for example shows the quantile prediction based on the fitted Type III exceedance probability model (without confidence bounds). Interestingly Fig. 1c very clearly confirms that the random data is indeed bounded from above by the value $|H_y(i\omega_r)| = 10$. However, similar results are in general less easy to interpret for mdof systems unless a deterministic bound is available. Moreover a fitted Type III model based on one sample size cannot be confidently used to make FRF bounding predictions. The potential use of a Type I model will, however, now be explored further on a small mdof structure namely a small grillage model.

3.1.2. *A small uncoupled mdof grillage model*

To begin to assess the suitability of the bounding method on a small mdof model, a small version of the grillage structure shown in Fig. 2 is examined. In general, the grillage in Fig. 2 comprises an $n \times n$ closed $x-y$ planar mesh of equispaced steel box-section beams. The model may be uncoupled, to represent the dynamics of the grillage structure, or it may be coupled to a cuboid cavity of air. An in-house research code was developed to perform FE analysis of both the uncoupled grillage and coupled systems. This code provided direct and complete control over the elements and solution process. A commercial FE code was not used initially because of the enormous amount of data exchange required for pre- and post-processing using rigid data formats, and because of licensing issues. The in-house code was verified with NASTRAN.

The small uncoupled model, comprising grillage beam elements of 0.5 m length, represents a 1.5 m × 1.5 m mesh with four longitudinal and four lateral beams fully clamped at their boundary, resulting in a model with 24 dof. The grillage beam cross-section has nominal dimensions: breadth $b = 0.0525\,\mathrm{m}$, height $h = 0.03\,\mathrm{m}$ and wall thicknesses t_{web} and t_{flange} equal to 0.001 m. The values for elastic and shear modulus $E = 210\,\mathrm{GN/m^2}$ and $G = 80.01\mathrm{GN/m^2}$ standard values for steel but the density $\rho = 27\,800\,\mathrm{kg/m^3}$ accounts for non-structural mass. Harmonic loading of fixed amplitude = 1 N, and a viscous damper with a nominal coefficient value $C = 200\,\mathrm{N\,s/m}$, are assumed to act in the z direction at node 6 (designated as grid 6–3). Two uncertain cases are examined: in the first case the box section beam dimensions h, t_{web}, and t_{flange} for each element, are treated as normal random variables with a COV value of 0.05 about their nominal values. In the second case, the viscous damper is additionally treated as uncertain, by assuming the damping coefficient C is a normal random variable also with a COV value of 0.05. In both cases 100 000 sample structures are generated as part of a Monte Carlo simulation and for each realisation the *inertance* FRF is constructed (i.e. acceleration/force).

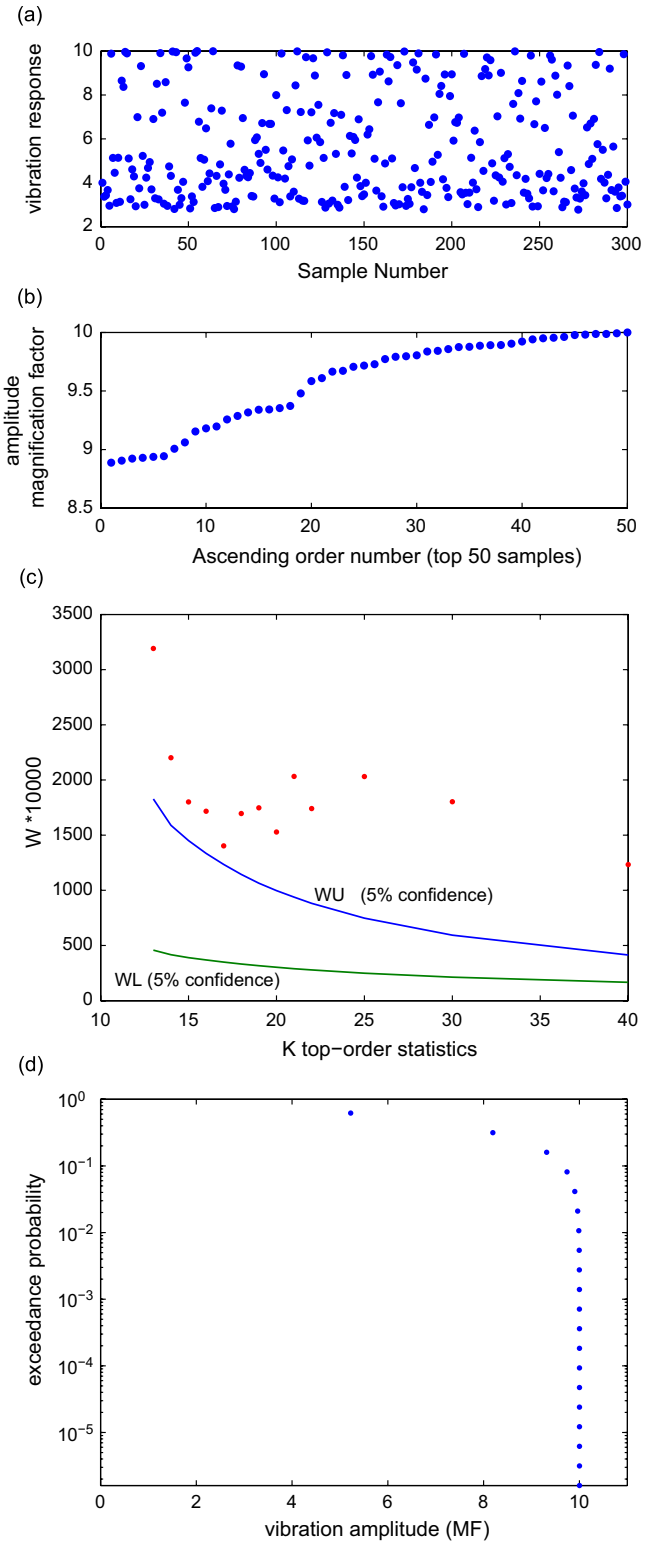

Fig. 1. (a) Top-order statistics; (b) ascending top-order statistics; (c) Hasofer–Wang test; and (d) a Type III quantile estimate for $\omega = 1.0$, $\mathrm{CoV}_k = 0.2$, $d_{\mathrm{crit}} = 0.05$.

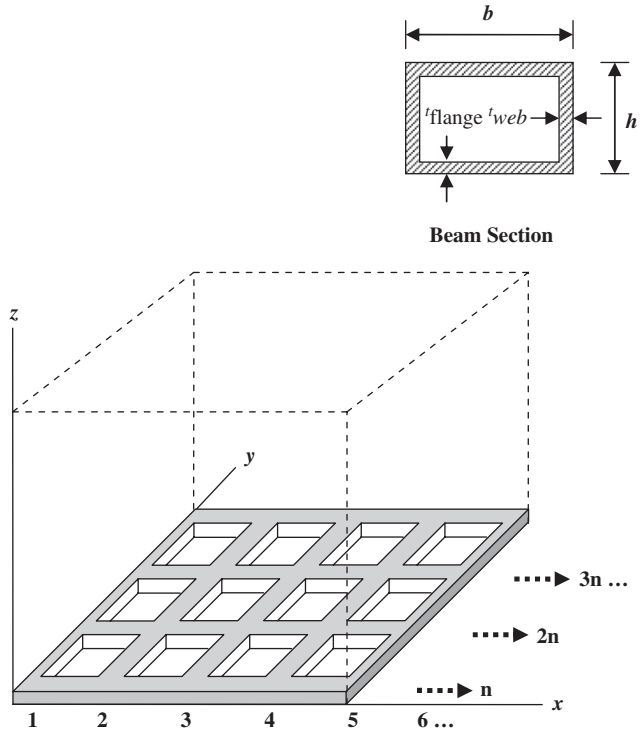

Fig. 2. A schematic view of an uncoupled grillage structure comprising a plane mesh of box-section beams showing the node numbering convention for an $n \times n$ mesh. When the grillage is coupled to a cuboid acoustic cavity, the grillage forms a flexible xy plane boundary.

The purpose of these test cases is to examine whether extreme FRFs at particular frequencies are Type I or not.

Fig. 3a shows, for the first case with fixed-damping, the FRFs for grid number 6–3 roughly spanning the first three resonant frequencies; Fig. 3b shows corresponding results for the second case where damping is additionally varied. The results of the Hasofer–Wang hypothesis test are shown in Fig. 4 at frequencies: 100, 110, 210, 290, and 325 Hz. The left-hand column of subplots corresponds to fixed damping; the right-hand column corresponds to random damping. The results in Fig. 4 clearly show that for fixed damping, extreme FRF data in the vicinity of (low) resonant frequencies is of Type III, whereas away from resonance it is of Type I. The resonant responses appear to be dominated by a single mode, which for fixed damping of this small uncoupled system, results in a clear physical bound. This can also be confirmed using the theoretical sdof *inertance* function near a natural frequency, which simplifies to $|H_{\ddot{y}}(\mathrm{i}\omega)| = \omega/C$. This is a linearly increasing bound on the resonant amplitude, which for a damping value $C = 200$ N s/m, has (in terms of frequency in Hz) a slope magnitude $= 2\pi/200$. As recommended in Section 2, and for the sdof model, when data is not of Type I, probabilistic bounds should not be attempted. With the introduction of normally distributed damping, however, the results are Type I thus supporting (attempted) application of the proposed bounding. But the more important immediate question is whether a deterministic bound is maintained for a larger uncoupled model without random damping.

3.1.3. A medium-sized uncoupled mdof grillage model

To assess whether the deterministic bound observed at resonance in the small structure is maintained when damping is fixed on a somewhat larger uncoupled structure, an extended version of the grillage model in Fig. 2 is examined. This larger grillage model represents a 5.5 m × 5.5 m mesh of 11 longitudinal and 11 lateral beams clamped on two opposite sides and free on the other two sides. The assessment now includes both hypothesis testing and FRF bounding via the *m-observational return level* discussed in Section 2. Bounds are predicted to correspond to two batch sizes of uncertain structure, namely a batch of 1000 and a batch of 10 000. To achieve

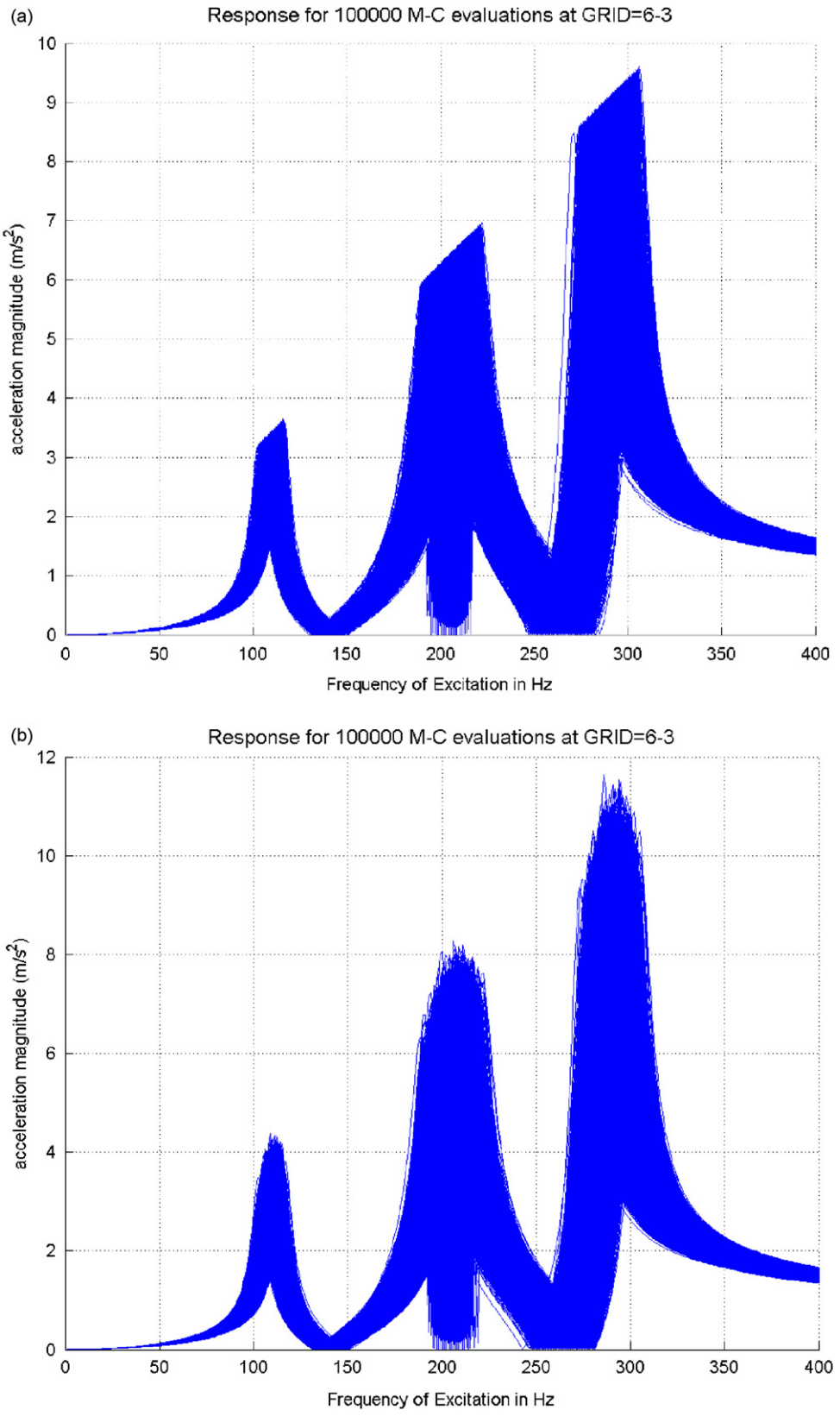

Fig. 3. (a) Inertance FRF for small uncoupled grillage model (without acoustic cavity) for fixed damping showing 100 000 realisations (GRID 6–3 refers to responses of node 6 in the z direction) and (b) inertance FRF for small uncoupled grillage model (without acoustic cavity) with normally distributed damping showing 100 000 realisations.

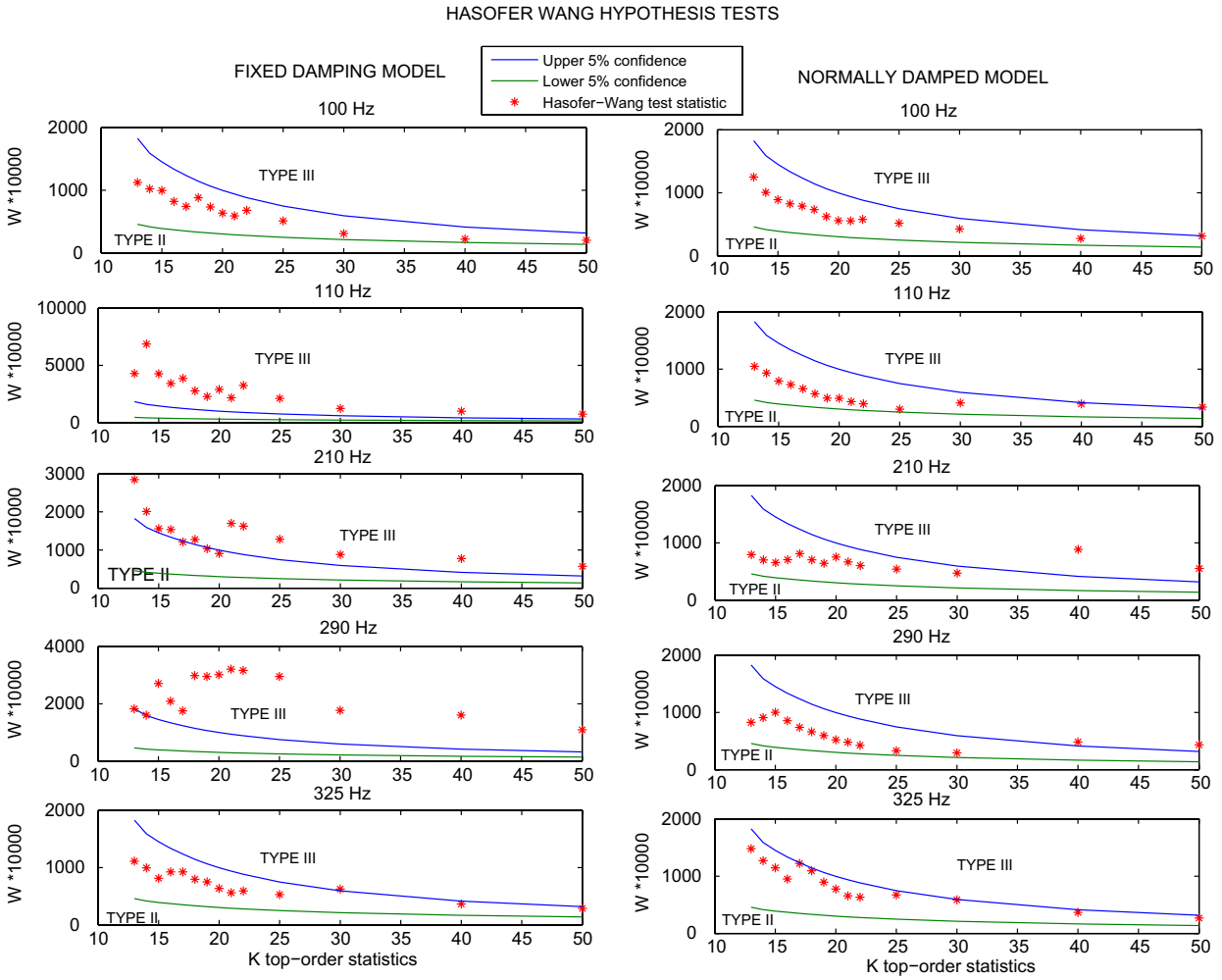

Fig. 4. Hasofer–Wang hypothesis test results at five frequencies for small-sized uncoupled grillage model with fixed and random damping.

this, two values of $m = 1000$ and 10 000 are used in a suitably justified Type I model which is fitted with $N_s = 100$. The samples are drawn at random but represent only a fraction of the values of m. Various statistics at a number of resonant frequencies associated with the predicted *m-observational return levels* based on a sample size of $N_s = 100$ are obtained shortly for comparison with statistics obtained directly from all the available maximum values. This includes, for the two values of m, direct estimation of the *m-observational return levels* from data generated by Monte Carlo simulation—which requires making use, respectively, of 20 000 and 200 000 structures, to allow in each case, the required averages to be computed using an adequate sample size (i.e. 20 values).

The nominal dimensions and material properties of the grillage are identical to the previous small mesh grillage except the width of the beam section is $b = 0.05$ m i.e. slightly reduced. Rayleigh damping proportional to mass and stiffness is assumed present across the entire structure, giving modal damping levels of 8 percent at 5 and 400 Hz. To introduce uncertainty in each element, the grillage beam dimensions b, h, t_{web}, and t_{flange} are treated as normal random variables with a CoV value of 0.05 about their nominal values.

Fig. 5 shows the Hasofer–Wang hypothesis test results at, or very near to, the eight lowest resonant frequencies, namely at: 12, 45, 65, 117, 166, 220, 247, and 330 Hz (in Fig. 7). Fig. 6 shows a corresponding single set of quantile predictions for various *m-observational return levels* (where the exceedance probability $p = 1/m$) and where approximate 2σ upper and lower confidence bounds are also shown. Fig. 7 shows the

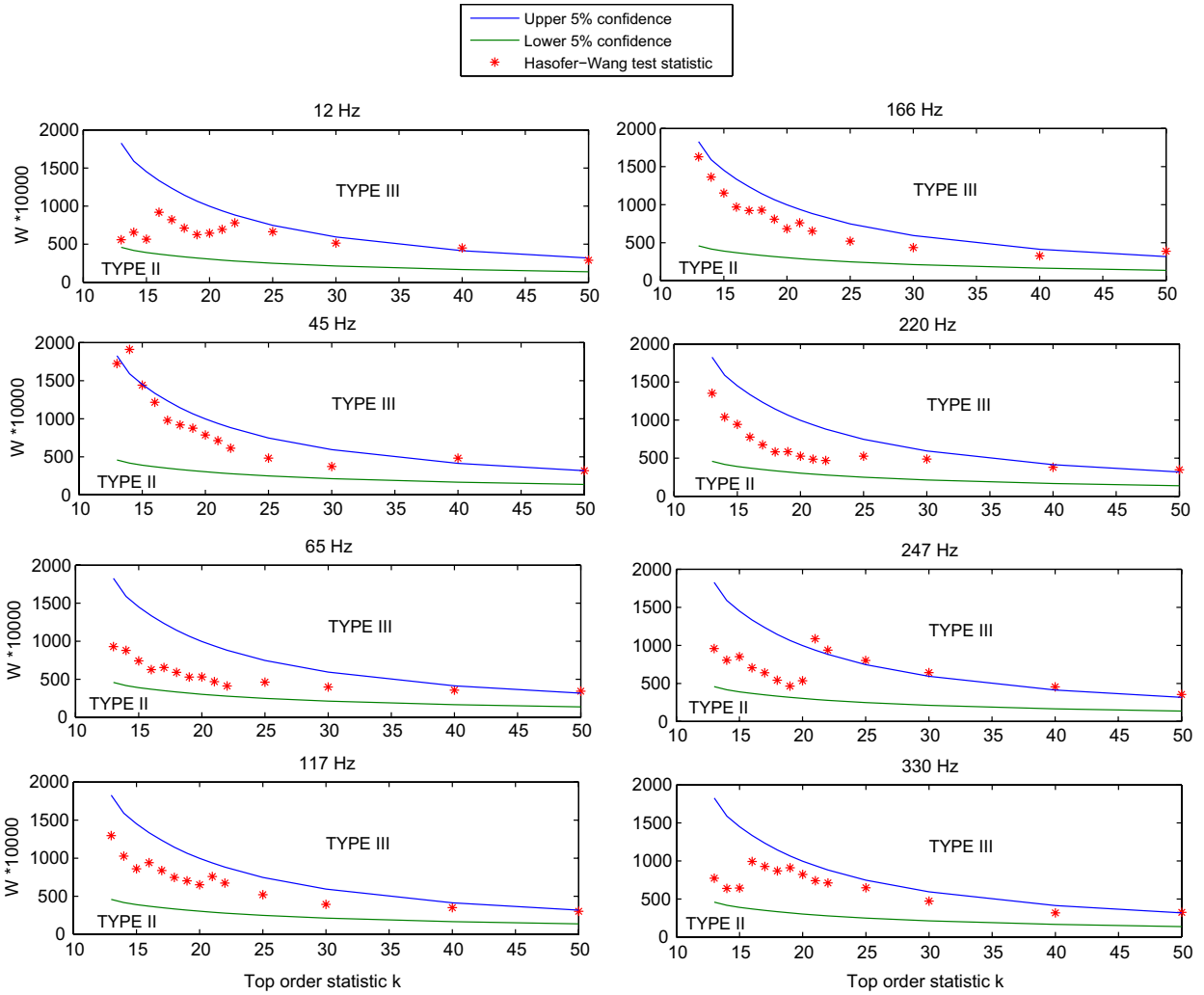

Fig. 5. Hasofer–Wang hypothesis test results at eight frequencies for medium-sized uncoupled grillage model.

nominal (inertance) FRF for the grillage spanning the eight frequencies, plus important results at each frequency for the two cases $m = 1000$ and 10 000, namely predicted FRF bound statistics along with directly measured maxima statistics. In particular Fig. 7a and b shows: (i) the mean value of 100 independent m-observational return level predictions based in each case on a sample size of $N_s = 100$ structures; (ii) the corresponding mean of the 100 predicted bounds $\pm 2\sigma$ levels; (iii) a single FRF bound prediction (as an example); and (iv) the directly measured m-observational return level using, respectively, 20×1000 and $20 \times 10\,000$ structures (which is also shown in Fig. 7c and d). Fig. 7c and d also shows the corresponding directly averaged maximum level, and the largest and smallest maximum in the sample of 20. First regarding the mean value of the predicted m-observational return level compared with the corresponding measured value, this comparison establishes whether predictions are biased. Fig. 7a and b does indeed show that there is a small conservative bias because the mean of the 100 predicted bounds appears to consistently exceed the directly measured m-observational return level (namely a comparison between the mean prediction shown with a '+' symbol and the direct measurement shown with a '×' symbol). A likely reason for this stems from the semi-empirical assignment of the threshold u via top-order statistics. Regarding the level of scatter in the 100 FRF bound predictions, the $\pm 2\sigma$ levels (shown with large '+' symbols) are very similar to the magnitudes of the constructed 2σ confidence intervals shown in Fig. 6. It is interesting to note that the directly measured

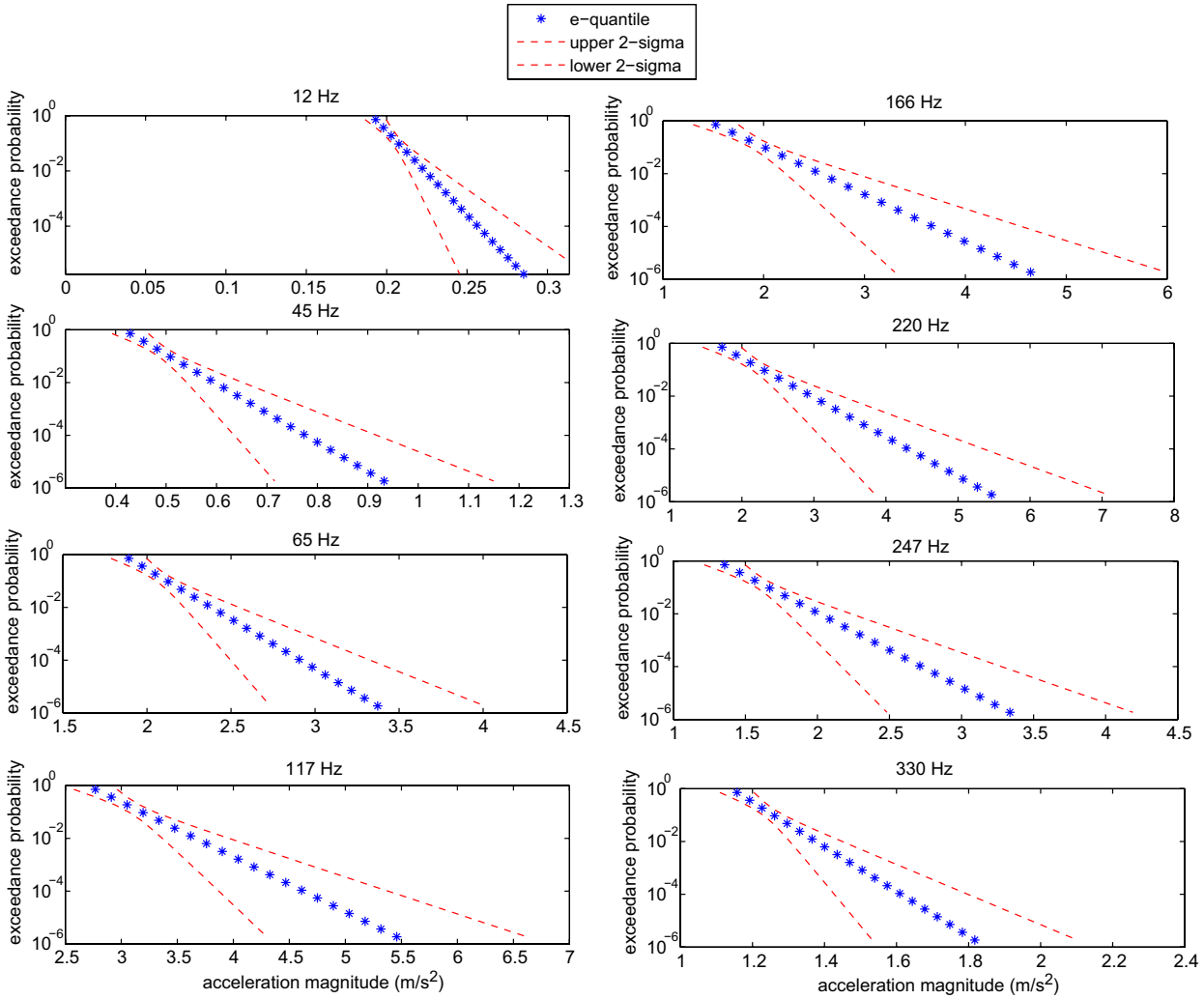

Fig. 6. Quantile prediction (m-observational return period for probability levels $= 1/m$) at eight frequencies for medium-sized uncoupled grillage model.

m-observational return level is very similar to the average maximum value (shown with a small '•' symbol). It is also evident from the largest and smallest maximum in the sample of 20 (shown with large '•' symbols) that there is apparent skew upwards, suggesting that most realised maxima would be near to the mean but occasionally a realisation may be substantially higher than the mean.

3.2. Scope and limitations

On the basis of the empirical evidence now available, some limitations of the method can be summarised. For a sdof system when damping is deterministic, the method will not produce Type I extremes at a resonant frequency because the response is totally independent of the mass and stiffness. Away from resonance, a sdof extreme response will, however, be Type I. With the introduction of random damping, sdof responses at a resonant frequency are Type I for normally distributed damping but a physical bound is still expected for uniformly distributed damping and therefore likely to be Type III. For small uncoupled mdof modal systems with deterministic damping, frequency responses around resonance also tend to be Type III, whereas away from resonance, Type I responses can be expected. For small uncoupled non-modal mdof systems with

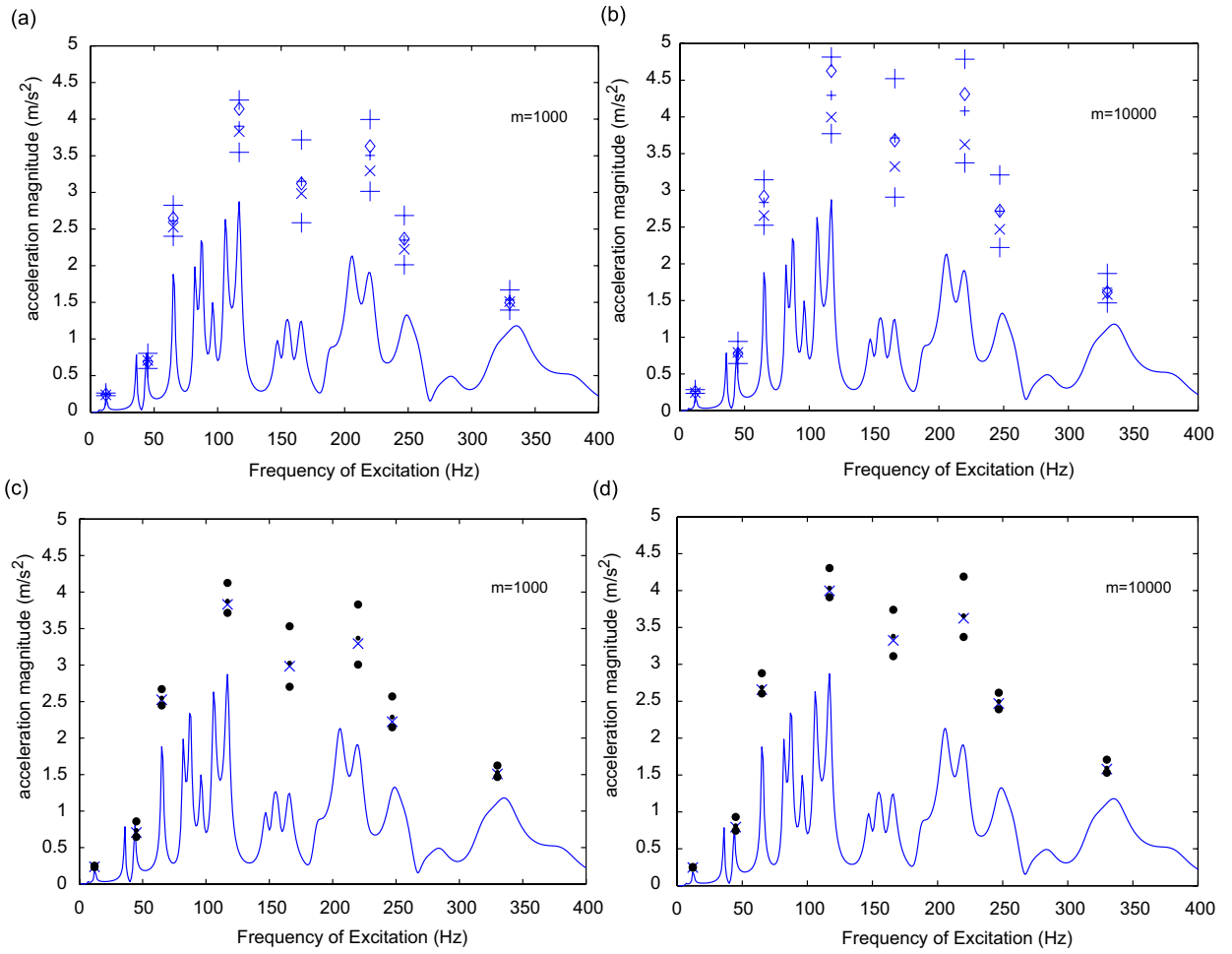

Fig. 7. Inertance FRF for (nominal) medium-sized uncoupled grillage at one location (−): (a) $m = 1000$ and (b) $m = 10\,000$ structures: + the mean value of 100 independent FRF-bound predictions at eight near-resonance frequencies i.e. the average m-observational return level obtained from 100 predictions, in each case based on a sample size of $N_s = 100$ structures; + the corresponding mean $\pm 2\sigma$ levels; ◇ a single FRF bound based on $N_s = 100$ structures; × the directly measured m-observational return level, also in (c) $m = 1000$, (d) $m = 10\,000$ structures: '·' the direct average maximum level; and '●' the largest and smallest maximum in the sample of 20 (both direct averages obtained using 20×1000 and $20 \times 10\,000$ structures, respectively).

deterministic damping, frequency responses around resonance may be Type I but the HW test is needed to confirm this. Away from resonance, for small non-modal, and modal systems with deterministic damping, Type I responses can be expected. For increasingly large uncoupled modal systems, even with deterministic damping, responses away from resonant peaks are very likely to be Type I, but responses around resonant peaks also appear to tend towards Type I even at low frequencies. Responses of the same structure coupled to an acoustic cavity are then even more likely to be Type I. This is because the participation of the structural modes provides additional randomisation of the acoustic peaks. The comparison in Fig. 7 confirms that the mean value of the predicted FRF bounds is moderately conservative, with a small consistent bias above the true m-observational return level. It should be noted that for structures with viscous damping (i.e. non-modal systems) or for structures coupled to an acoustic cavity, none of the available methods appear suitable for predicting bounds. Moreover, unlike virtually all existing alternatives, the proposed method can be applied directly to data obtained from real structures.

The proposed method is therefore in principle applicable to any structural dynamic response whether predicted using a model or using measured data from a real structure, in which the responses can be deemed to

be stationary, and independent identically distributed (i.i.d.) random variables. The basis of the method is to assume that the EVs of finite samples can be modelled using an asymptotic threshold exceedance model. In practice, as with all statistical methods, predictions are prone to scatter, therefore the main issues are concerned with knowing in advance precisely how much data is needed, collecting sufficient data of the correct type, and then drawing the appropriate inferences from the data. The proposed method does, however, have the capability of constructing reliable confidence intervals which clearly indicate how the sample size N_s influences the scatter in the predicted bounds.

3.3. Computational efficiency

Regarding computational efficiency, there are two important issues. The first concerns the efficiency of the method compared to alternative bounding methods. The second issue concerns the efficiency gains obtained by exploiting asymptotic threshold models to construct quantile estimates. Regarding alternative bounding approaches, existing methods are generally suited to relatively small modal systems, therefore it is quite possible that on small systems the proposed method offers no computational advantages given that data must be generated via Monte Carlo simulation of a representative sample of structures. However, for application to larger systems existing alternatives search for bounds that may occur with extremely low probabilities, and in so doing expend substantial computational effort to obtain a result of limited practical relevance.

Regarding the efficiency derived from using threshold models to estimate the *m-observational return level*, the first point of note is that compared to Monte Carlo simulation the computational effort needed for the HW hypothesis test and the *return level* prediction via the Weissman estimator is almost negligible. Predictions are made corresponding to a batch of uncertain structures of size *m,* which typically might be 10–100 times larger than N_s. But to directly measure the *m-observational return level*, a substantially larger batch size is needed (around 20 times the batch size) so the prediction efficiency rather than being 10–100 fold is in fact more like 200–2000 fold. It is precisely this kind of speed advantage that makes the method attractive for bounding large models coupled to an acoustic cavity where Monte Carlo simulations are significantly more demanding than for uncoupled structures. Applications will now focus on coupled structures.

4. Application to a grillage with random structural properties coupled to an acoustic cavity

To test the FRF bounding method on a medium-scale structure coupled to an acoustic air cavity, an FE model of the grillage base shown in Fig. 2 is now used with appropriate modification. The *l*, *b*, *d* dimensions of the block of air are $2\,\mathrm{m} \times 1.5\,\mathrm{m} \times 1\,\mathrm{m}$ (roughly the size of an acoustic cavity in the passenger space of a small vehicle). The outer air boundary is *hard* whereas the interior boundary is connected to the flexible grillage base. The grillage beam elements are fixed at the boundary. NASTRAN-type bar elements are adopted. Bending plate FEs are used to couple the grillage structure to the air volume using a consistent coupling. The theoretical basis is drawn directly from [36] with detailed reference to the theory in [37–39]. By industry standards this 'larger' fluid–structure grillage model, with approximately 1500 dofs, is small. Again, the in-house code was used for the analyses with totally random parameter control and simplified pre- and post-processing. For analysis of large FE structures (as examined in Section 5) use of commercial software is necessary. The extended version of Eq. (1) including fluid loading is given as

$$[\mathbf{M}_s]\ddot{\mathbf{Y}} + [\mathbf{D}_s]\dot{\mathbf{Y}} + [\mathbf{K}_s]\mathbf{Y} = \mathbf{L}_e + \mathbf{L}_f \tag{27}$$

where $[\mathbf{M}_s]$, $[\mathbf{D}_s]$, and $[\mathbf{K}_s]$ are structural mass, damping, and stiffness matrices, $\mathbf{L}_e$ is the externally applied load, and $\mathbf{L}_f$ is the nominal fluid load on the structure. By following the procedure in [36], Eq. (27) can be assembled into an explicit system of coupled fluid–structure equations of motion as follows:

$$\begin{bmatrix} \mathbf{M}_s & \mathbf{0} \\ \mathbf{0} & -\mathbf{M}_f \end{bmatrix} \begin{bmatrix} \ddot{\mathbf{Y}} \\ \ddot{\mathbf{Q}} \end{bmatrix} + \begin{bmatrix} \mathbf{D}_s & \mathbf{C} \\ \mathbf{C}^T & \mathbf{0} \end{bmatrix} \begin{bmatrix} \dot{\mathbf{Y}} \\ \dot{\mathbf{Q}} \end{bmatrix} + \begin{bmatrix} \mathbf{K}_s & \mathbf{C} \\ \mathbf{0} & -\mathbf{K}_f \end{bmatrix} \begin{bmatrix} \mathbf{Y} \\ \mathbf{Q} \end{bmatrix} = \begin{bmatrix} \mathbf{L}_e \\ \mathbf{0} \end{bmatrix} \tag{28}$$

where $\mathbf{Q}$ is a time-integrated pressure vector, $\mathbf{M}_f$ and $\mathbf{K}_f$ are respective fluid mass and stiffness matrices, and $\mathbf{C}$ is a coupling matrix.

Reduction in the size of the model Eq. (28) may be obtained using modal reduction by assuming a reduced set of eigenvectors is calculated for the structure and fluid by solving:

$$[\mathbf{K}_s - \lambda_s \mathbf{M}_s]\mathbf{\Phi}_s = [\mathbf{0}] \tag{29}$$

and

$$[\mathbf{K}_f - \lambda_f \mathbf{M}_f]\mathbf{\Phi}_f = [\mathbf{0}] \tag{30}$$

where $\mathbf{\Phi}$ is the reduced modal matrix. The displacement and pressure is then assumed to be a linear summation of eigenvectors as follows:

$$\mathbf{Y} = \mathbf{\Phi}_s \xi_s \tag{31}$$

and

$$\mathbf{P} = \mathbf{\Phi}_f \xi_f \tag{32}$$

where ξ_s and ξ_f are respective structure and fluid modal coordinate vectors. On substitution of Eqs. (31) and (32) into (28) and pre-multiplying each row by either the structure or fluid eigenvectors as appropriate, the

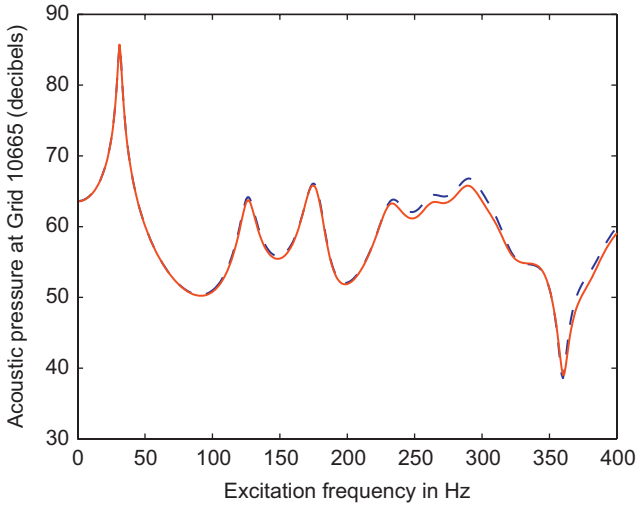

Fig. 8. Acoustic response from coupled grillage: NASTRAN model: ——; 'in-house' model: – – –.

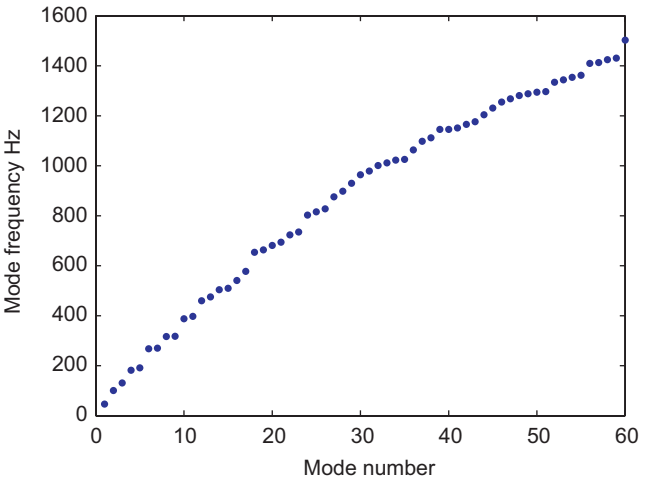

Fig. 9. Baseline mode frequencies for the grillage structure.

following system is obtained:

$$\begin{bmatrix} \mathbf{m}_s & \mathbf{0} \\ \mathbf{0} & -\mathbf{m}_f \end{bmatrix} \begin{bmatrix} \ddot{\boldsymbol{\xi}}_s \\ \ddot{\boldsymbol{\xi}}_f \end{bmatrix} + \begin{bmatrix} \mathbf{d}_s & \boldsymbol{\zeta}^{\mathrm{T}} \\ \boldsymbol{\zeta} & \mathbf{0} \end{bmatrix} \begin{bmatrix} \dot{\boldsymbol{\xi}}_s \\ \dot{\boldsymbol{\xi}}_f \end{bmatrix} + \begin{bmatrix} \mathbf{k}_s & \mathbf{0} \\ \mathbf{0} & -\mathbf{k}_f \end{bmatrix} \begin{bmatrix} \boldsymbol{\xi}_s \\ \boldsymbol{\xi}_f \end{bmatrix} = \begin{bmatrix} \mathbf{f}_s \\ \mathbf{0} \end{bmatrix} \tag{33}$$

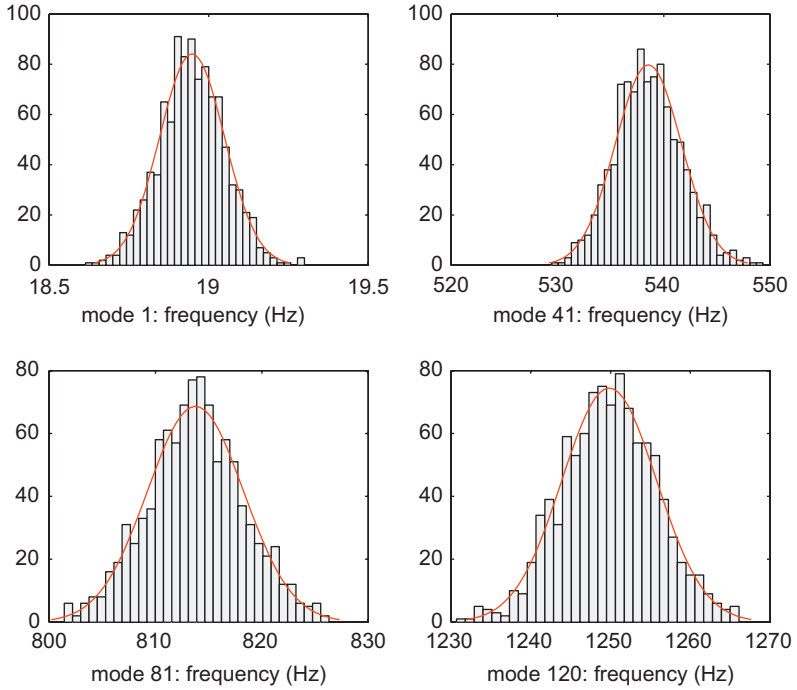

Fig. 10. Distributions of mode frequencies for randomised grillage structure.

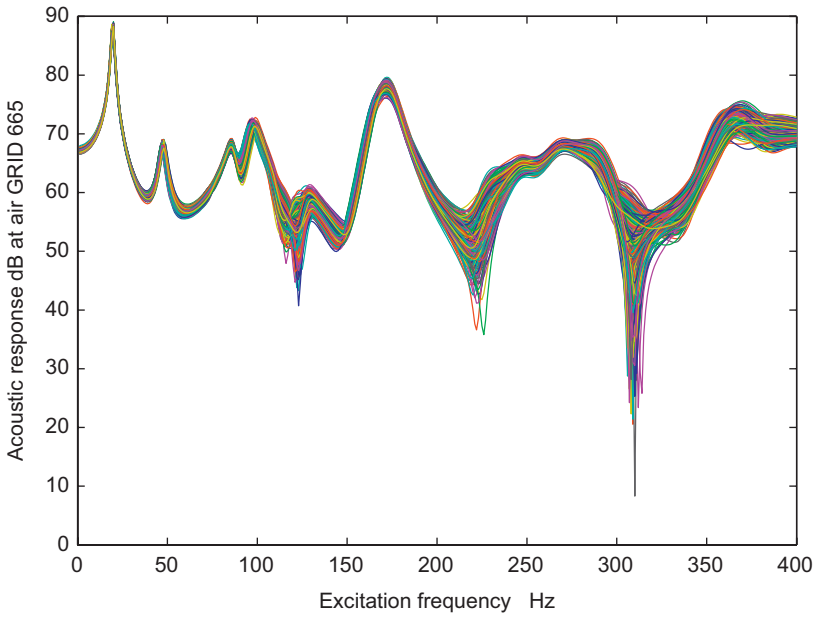

Fig. 11. Acoustic FRF (SPL Response) at GRID 665-standard modal analysis (new modes) with 1000 runs.

The respective terms in Eq. (33) are given by the set of equations:

$$\mathbf{m}_s = \mathbf{\Phi}_s^{\mathrm{T}} \mathbf{M}_s \mathbf{\Phi}_s \tag{34}$$

$$\mathbf{d}_s = \mathbf{\Phi}_s^{\mathrm{T}} \mathbf{D}_s \mathbf{\Phi}_s \tag{35}$$

$$\mathbf{k}_s = \mathbf{\Phi}_s^{\mathrm{T}} \mathbf{K}_s \mathbf{\Phi}_s \tag{36}$$

$$\mathbf{f}_s = \mathbf{\Phi}_s^{\mathrm{T}} \mathbf{L}_{\mathbf{e}} \tag{37}$$

$$\mathbf{m}_f = \mathbf{\Phi}_f^{\mathrm{T}} \mathbf{M}_f \mathbf{\Phi}_f \tag{38}$$

$$\mathbf{k}_f = \mathbf{\Phi}_f^{\mathrm{T}} \mathbf{K}_f \mathbf{\Phi}_f \tag{39}$$

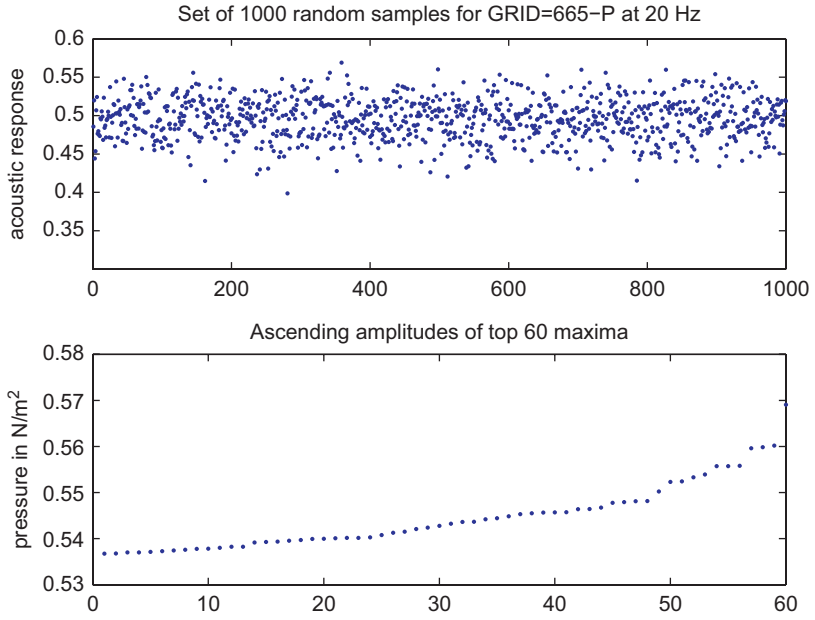

Fig. 12. Top-order statistics at 20 Hz for $N_s = 1000$ for acoustic response at location 665.

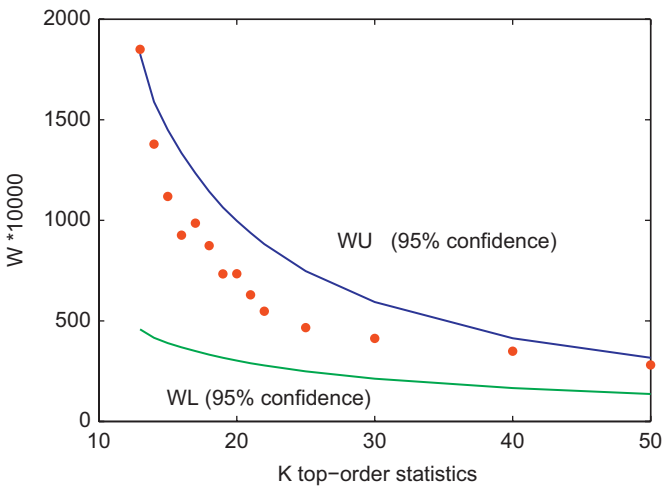

Fig. 13. Hasofer–Wang test at 20 Hz for $N_s = 1000$ for acoustic response at location 665.

Finally, a fluid modal damping matrix $\mathbf{d}_f$ is introduced to the reduced system as a mathematical device to model energy dissipation. The fluid–structure modal Eq. (31) then becomes:

$$\begin{bmatrix} \mathbf{m}_s & \mathbf{0} \\ \mathbf{0} & -\mathbf{m}_f \end{bmatrix} \begin{bmatrix} \ddot{\xi}_s \\ \ddot{\xi}_f \end{bmatrix} + \begin{bmatrix} \mathbf{d}_s & \zeta^{\mathrm{T}} \\ \zeta & -\mathbf{d}_f \end{bmatrix} \begin{bmatrix} \dot{\xi}_s \\ \dot{\xi}_f \end{bmatrix} + \begin{bmatrix} \mathbf{k}_s & \mathbf{0} \\ \mathbf{0} & -\mathbf{k}_f \end{bmatrix} \begin{bmatrix} \xi_s \\ \xi_f \end{bmatrix} = \begin{bmatrix} \mathbf{f}_s \\ \mathbf{0} \end{bmatrix} \tag{40}$$

The in-house code implementing the model Eq. (40) has been verified using a NASTRAN model in both static and dynamic cases. The model is solved over a frequency range of 400 Hz using a conventional modal reduction with 120 structural and 350 fluid modes. Modal damping levels of 4 percent critical are assumed for both air and structure, along with standard engineering material properties for air and steel. For the assembled air block and coupling elements, under a variety of load conditions, responses are in excellent agreement with NASTRAN up to around 220 Hz. Fig. 8 shows an example comparison for unit harmonic load applied at a position offset from the centre of the grillage base, where the acoustic FRF (in decibels) is predicted at the

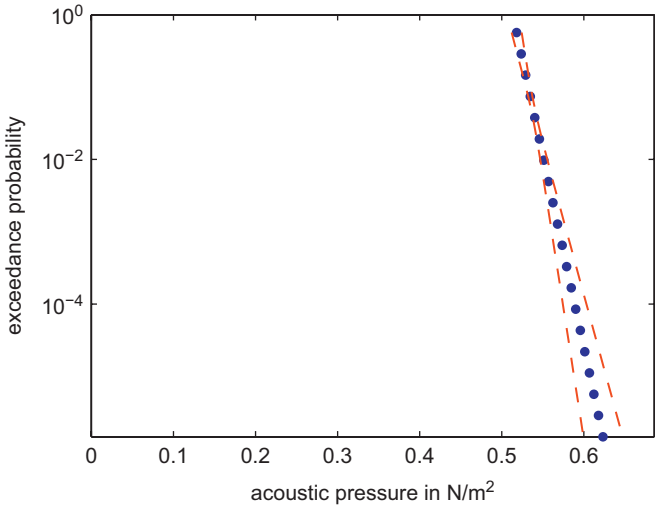

Fig. 14. Weissman quantile estimate at 20 Hz for $N_s = 1000$ for acoustic response at location 665.

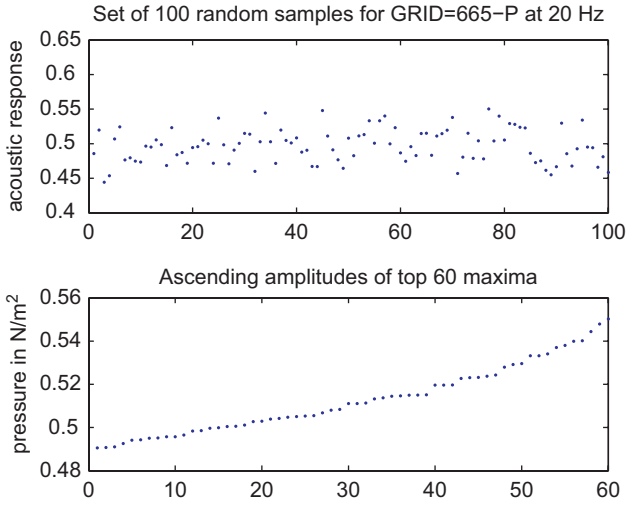

Fig. 15. Top-order statistics at 20 Hz for $N_s = 100$ for acoustic response at location 665.

centre of the block of air. Beyond 220 Hz, small differences appear owing to the use of consistent coupling in the grillage code. These differences are of no concern here. Fig. 9 shows the mode frequencies of the grillage base structure used in the verification analysis. For the data generation described in the following a significant adjustment is made to the density of the steel used for grillage beams in order to increase the number of modes in low frequency region. (Note in respect of Fig. 9, it is strictly not appropriate for a randomly uncertain structure, to associate specific eigenvalues with modes since in general, the Nth frequency in each realisation will correspond to a different mode.)

Sample acoustic FRFs are now generated using this grillage model to test the extreme-value-based FRF bounding method of Section 2. Monte Carlo simulations of acoustic FRFs are performed with fully random geometry and material properties for each structural FE. In particular, the dimensions of the beam section h, and b, the web thickness t_{web}, the flange thickness t_{flange}, Young's modulus E, and the steel density ρ_s, are all generated for each realisation by sampling from independent normal distributions, with coefficients of variation = 0.05. The nominal values are $h = 30$ mm, $b = 20$ mm, $t_{\text{web}} = 2$ mm and $t_{\text{flange}} = 2$ mm. The applied load, and the response location is kept fixed throughout (i.e. the chosen 'GRID' point defining the fluid

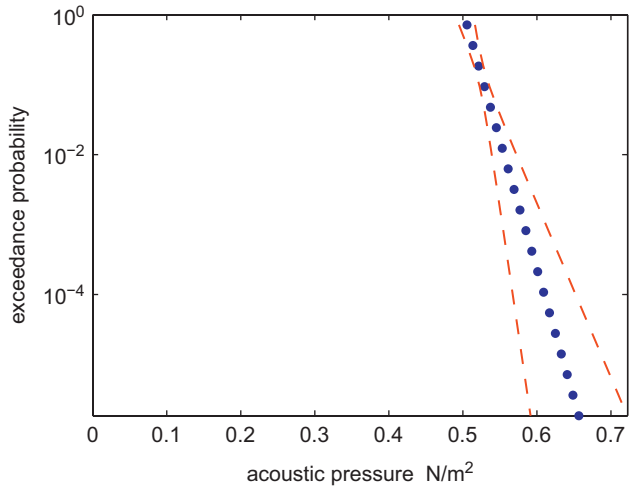

Fig. 16. Weissman quantile estimate at 20 Hz for $N_s = 100$ for acoustic response at location 665.

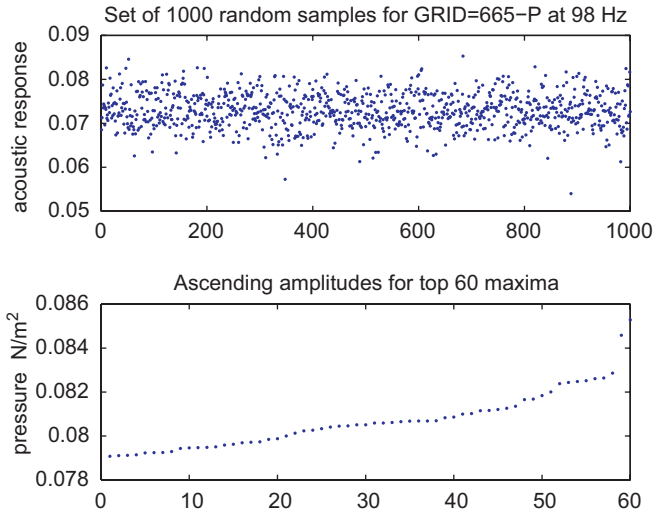

Fig. 17. Top-order statistics at 98 Hz for $N_s = 1000$ for acoustic response at location 665.

element node location for calculating the response is kept fixed). The excitation frequency is increased in steps of 1 Hz to a maximum of 400 Hz. In total, 1000 simulation runs are made at each frequency using standard modal frequency response analysis, where structural modes are calculated for each realisation. Again a total of 120 structural modes, and 350 fluid modes are used in the FRF calculations, assuming standard properties for air (i.e. velocity of sound $c = 344\,\mathrm{m/s}$, and density $\rho_a = 1.2\,\mathrm{kg/m^3}$), and fixed viscous modal damping at 4 percent for both fluid and structure.

Fig. 10 shows four histograms for selected modes giving the distribution of modal frequencies (suggesting these are approximately normal). The corresponding mean frequencies are lower than those shown in Fig. 9 owing to the use of higher density steel in the grillage beams. The ensemble of acoustic FRFs (at location GRID 665) is shown in Fig. 11. Two low-frequency resonance conditions are selected for the test namely at 20 and 98 Hz. Fig. 12 shows the 20 Hz raw data for the entire 1000-structure acoustic response ensemble and a corresponding number of 60 top-order statistics. Fig. 13 shows the Hasofer–Wang test using Eq. (24). Fig. 14 shows the quantile prediction using the Weissman Type I Eq. (20) i.e. for $N_s = 1000$ (based on the recommended top-order statistic value $k = 1.5\sqrt{N_s}$) along with approximate two standard deviation

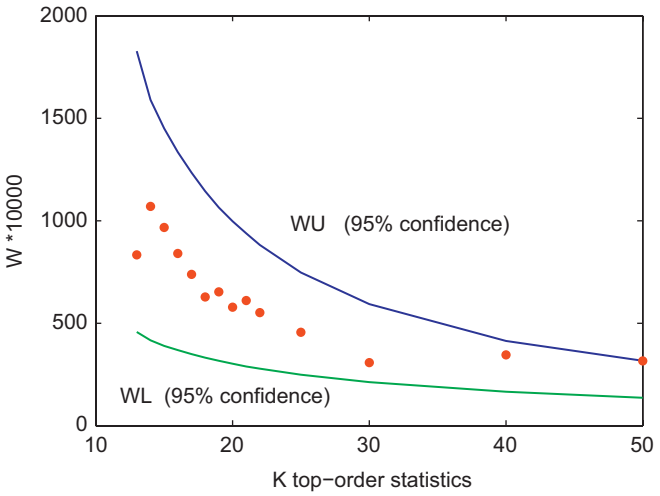

Fig. 18. Hasofer–Wang test at 98 Hz for $N_s = 1000$ for acoustic response at location 665.

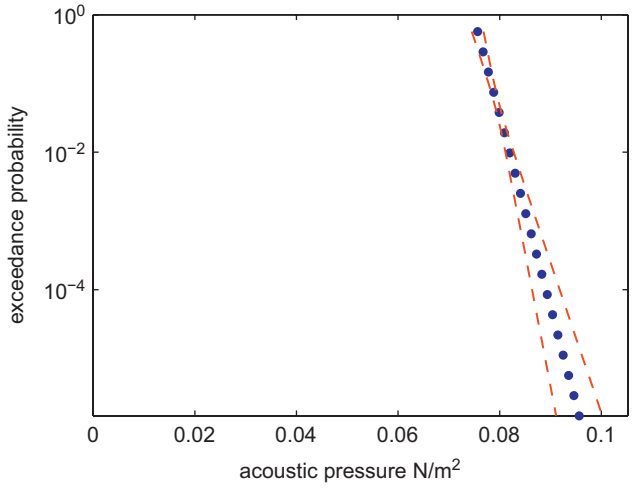

Fig. 19. Weissman quantile estimate at 98 Hz for $N_s = 1000$ for acoustic response at location 665.

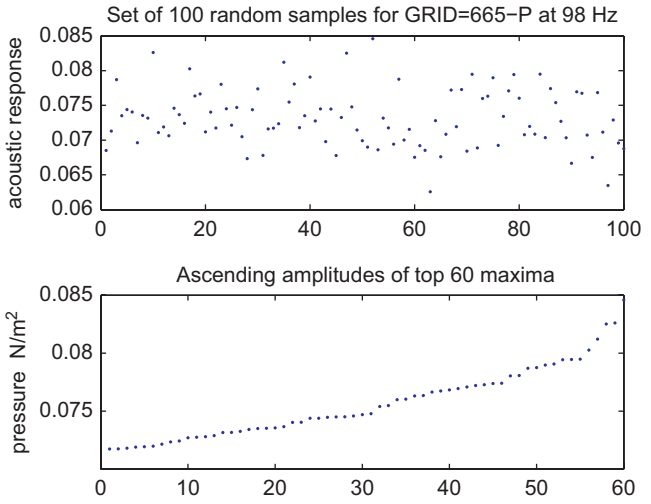

Fig. 20. Top-order statistics at 98 Hz for $N_s = 100$ for acoustic response at location 665.

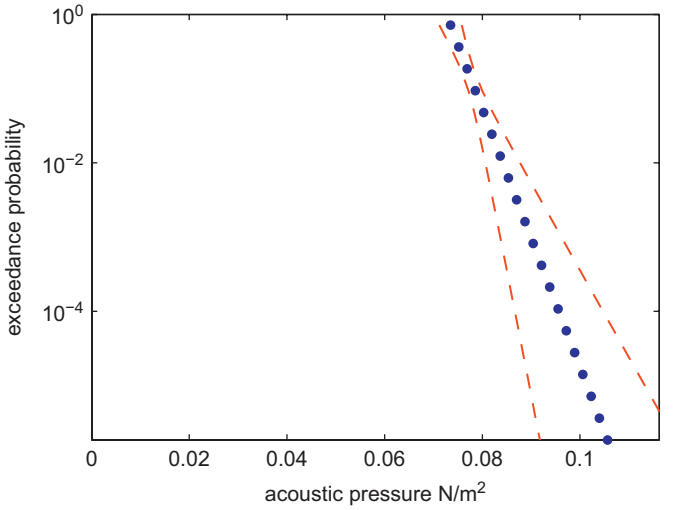

Fig. 21. Weissman quantile estimate at 98 Hz for $N_s = 100$ for acoustic response at location 665.

confidence intervals constructed using Eq. (22). Fig. 15 shows the same 20 Hz raw data and top-order statistics but for a reduced random sample of 100-structures. Fig. 16 shows the corresponding reduced-ensemble-based quantile prediction for $N_s = 100$ using the Weissman Type I Eq. (20), also including confidence intervals.

Figs. 17–19, respectively, show the 98 Hz raw data and top-order statistics, the Hasofer–Wang test results, and the Weissman Type I quantile predictions, for $N_s = 1000$ i.e. using the entire 1000-structure acoustic response ensemble. Fig. 20 shows the 98 Hz raw data and top-order statistics for a randomly reduced sample of 100-structures. Fig. 21 shows the corresponding 98 Hz reduced-ensemble-based quantile prediction using the Weissman Type I Eq. (20) i.e. for $N_s = 100$.

4.1. Discussion of results for the random grillage coupled to an acoustic cavity

The Hasofer–Wang hypothesis test results in Figs. 13 and 18 provide substantial justification for use of the 'unbounded' Weissman quantile estimator for Type I. In fact, at all of the frequencies examined, use of the type I estimator was justified by the HW test in all cases. This implies that statistically, this data is not

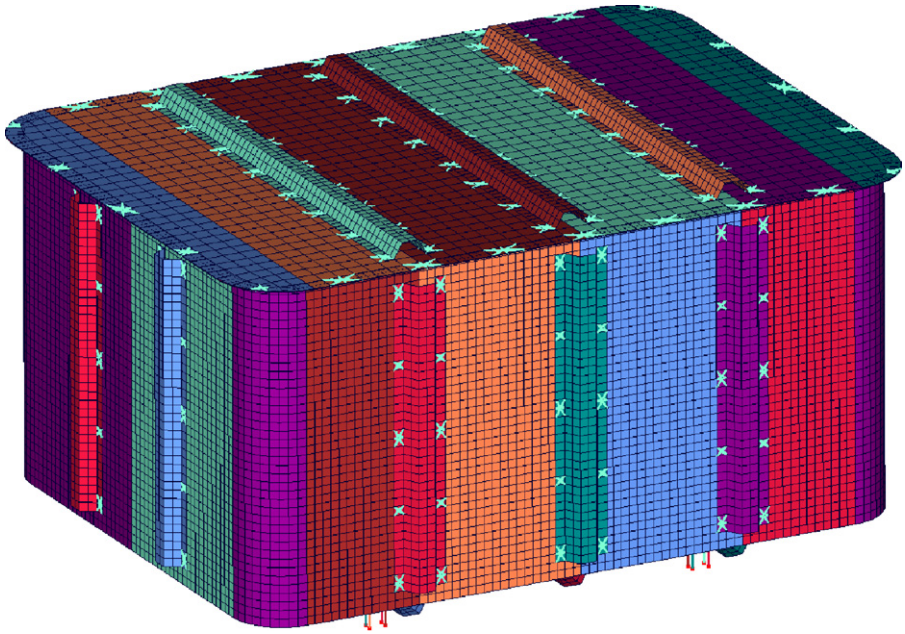

Fig. 22. Finite element model of box structure showing plate variables.

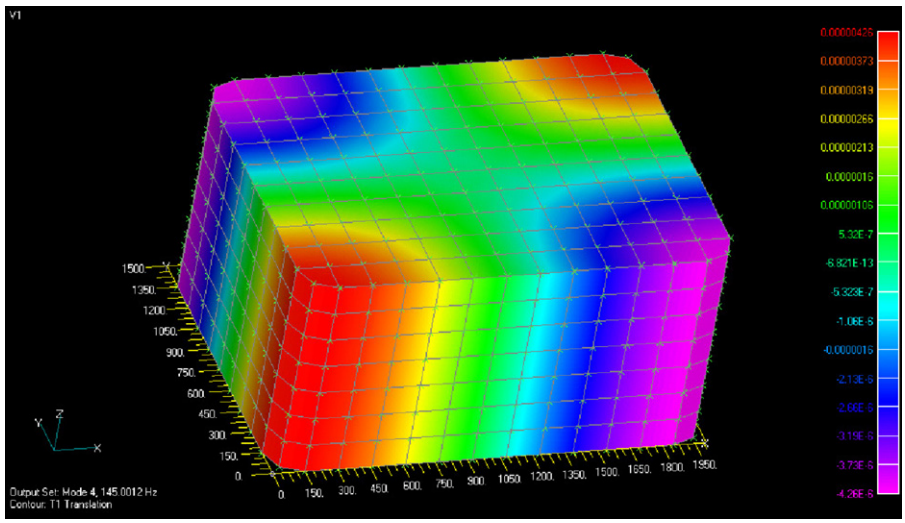

Fig. 23. Finite element model of air cavity showing mode shape.

bounded even though a physical bound does exist. Regarding quantile predictions using the Weissman estimator, the prime interest is in assessing whether quantile estimates using relatively few data samples compare well with actual extreme acoustic responses observed in a larger data set. For the 20 Hz resonant condition, Fig. 16 (using $N_s = 100$ randomly selected samples) compared with Fig. 14 (using $N_s = 1000$ randomly selected samples) shows that quantile estimates at a probability level $p = 1/m = 10^{-3}$, for $m = 1000$, are very similar to the maximum observed in Fig. 12. For the 98 Hz resonant condition, Fig. 21 (again using $N_s = 100$ randomly selected samples) compares well with Fig. 19 (using $N_s = 1000$ randomly selected samples) again marginally exceeding the actual maximum response (Fig. 17). These successful applications of the Weissman Type I estimator to this large grillage structure now provides strong motivation to apply the method to an industrial scale problem.

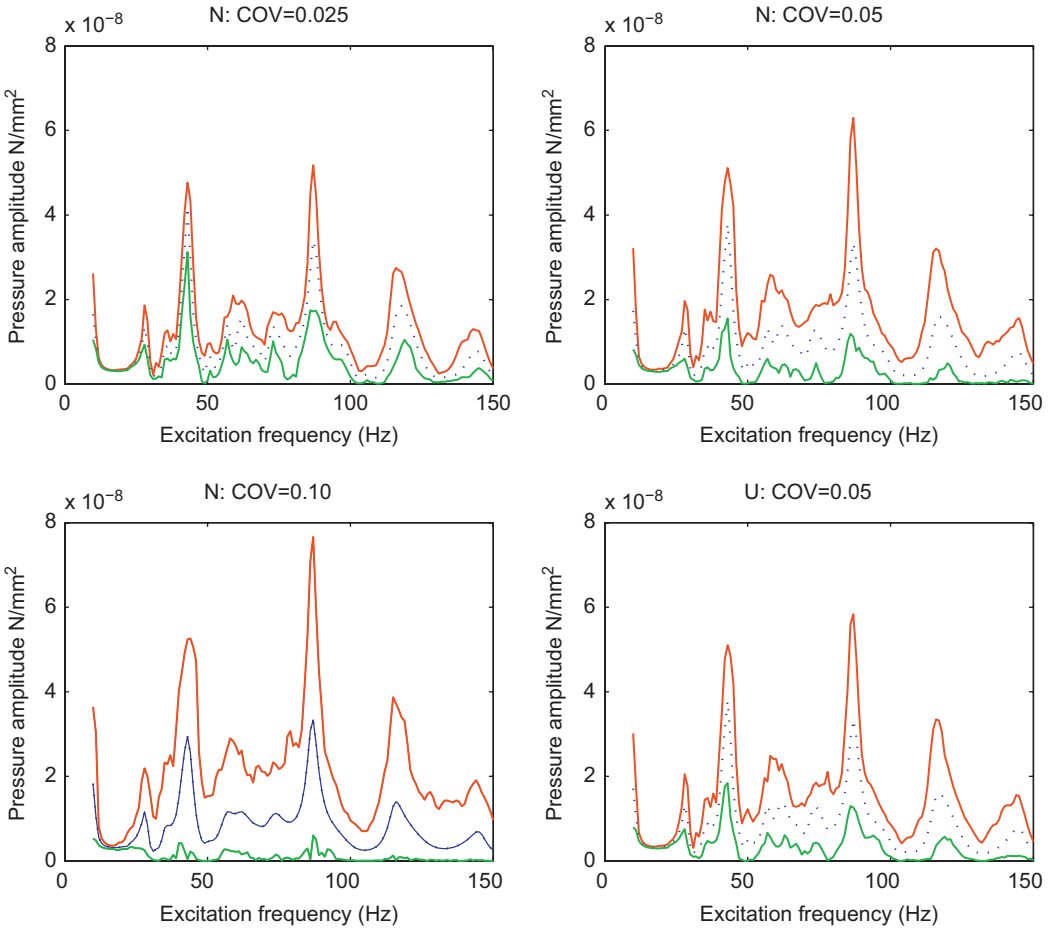

Fig. 24. Acoustic pressure FRF minimum, maximum, and mean for dof 9001032 with normal and uniform distributions. Minimum ——; maximum ——; mean ·····.

5. FRF bounding for an industrial-scale random box model

With the apparent success in Section 4 of using a suitable type I quantile estimator for FRF bounding at a number of discrete resonant conditions, an industrial-scale model is now considered [40] for further testing across the entire frequency range. A box-structure containing an acoustic cavity is chosen since this exhibits many of the dynamic characteristics of a small vehicle body. The thicknesses of 42 plate components are defined as probabilistically uncertain variables. And to provide a set of benchmark results by which the frequency response bounding method of Section 2 can be assessed, a total of 8000 FRF calculations are performed using NASTRAN (requiring around 2500 CPU hours in total on high performance workstations).

First the model is described, followed by a description of the cavity. Fig. 22 shows the FE model of a closed stiffened-steel box structure with overall dimensions (2 m × 1.5 m × 1 m). This structure is attached to ground using four damped spring mounts with stiffness values similar to those used to attach a vehicle body to its suspension system. The structural FE model was created (using the mesh generation programme FEMAP) and has over 100 000 dof. The box structure comprises plate components (including stiffeners) with a nominal thickness of 2 mm. This is the nominal or 'baseline' structure. Individual plate fields are connected by seam welds. The stiffeners attached to the exterior of the box are connected to the flat plate structure by spot welds. (The spot weld modelling was achieved with CDH/SPOT, which is widely used software in the automobile industry for creating vehicle-body FE models from separately meshed plate components). Fig. 23 shows the

FE model for the air cavity. The 'air' model was also constructed using FEMAP. Also shown on Fig. 23 is a contour plot of modal pressure distribution for mode 4. This model exhibits many of the dynamic characteristics of a vehicle body enclosing a passenger compartment air cavity. The model contains many structural mode frequencies within the acoustic frequency of interest and is therefore considered to represent a medium-sized industrial vehicle body model suitable for testing the method of Section 2.

Turning to the specifics of the FRF calculations, a harmonic force of 1 Newton is applied at a point offset from the centre on the base. The frequency response is considered of some 30 arbitrarily selected structural dofs and two air cavity acoustic pressure positions (assuming this box were a vehicle, these locations would correspond approximately to driver and passenger ear positions). These responses are calculated in 1 Hz steps across the frequency range 10–150 Hz. The calculations were performed in fluid–structure modal frequency response analysis (SOL 111) in NASTRAN. Structural modes were calculated using the Lanczos algorithm [41]. Modes up to 350 Hz (554 modes for the nominal design) and 87 fluid-modes up to 600 Hz, were calculated and used to form the modal equations. In addition to the damping of the mounts, a low viscous modal damping (2 percent critical) was used for both structure and fluid. The physical coupling matrix between structure and fluid was calculated in MSC.NASTRAN V2005. To reduce calculation time in subsequent Monte Carlo calculations, the physical coupling matrix was calculated once only, and used repeatedly during subsequent calculations.

For the purpose of Monte Carlo simulation, the thicknesses of 42 uncertain plates were defined as uncorrelated random variables. In the generation of random variables, Gaussian probability density distributions were chosen to give COV values of 0.025, 0.05, and 0.1 for each variable. A single uniform distribution with COV value of 0.05 was also used. The figures are identified, respectively, with the letter N (for normal) or U (for uniform). For each of these four levels of variability, 2000 sets of 42 randomly generated plate thickness 'realisations' were generated. Thus a total of 8000 NASTRAN runs were performed at each frequency with a different set of plate thicknesses. Each of these 8000 NASTRAN runs involved a new modes calculation for the structure leading to a unique set of modal equations. Computations were performed on HP Itanium, IBM Power 5, and NEC Itanium servers (requiring 2500 CPU hours in total).

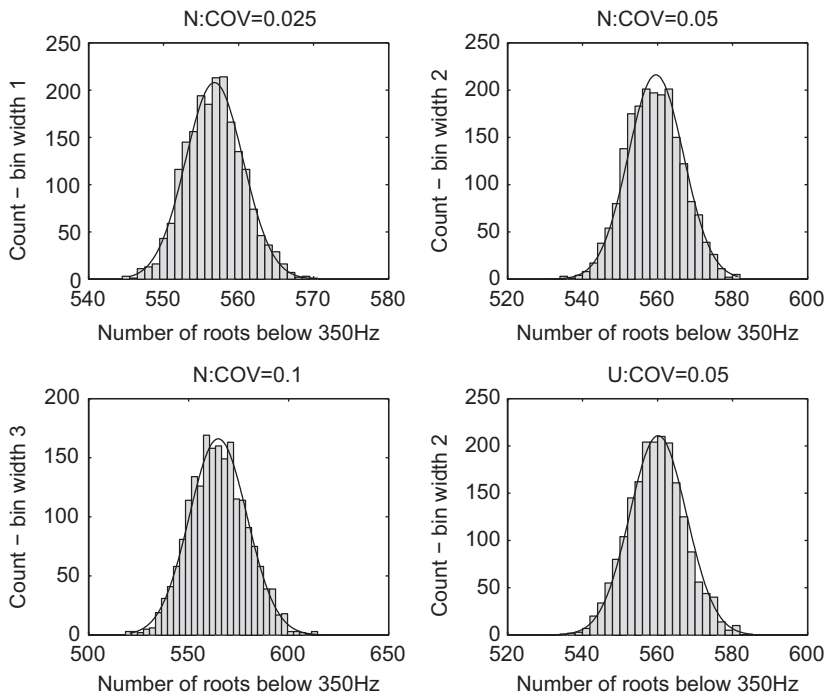

Fig. 25. Histograms of root-count below 350 Hz in 4×2000 Monte Carlo analyses.

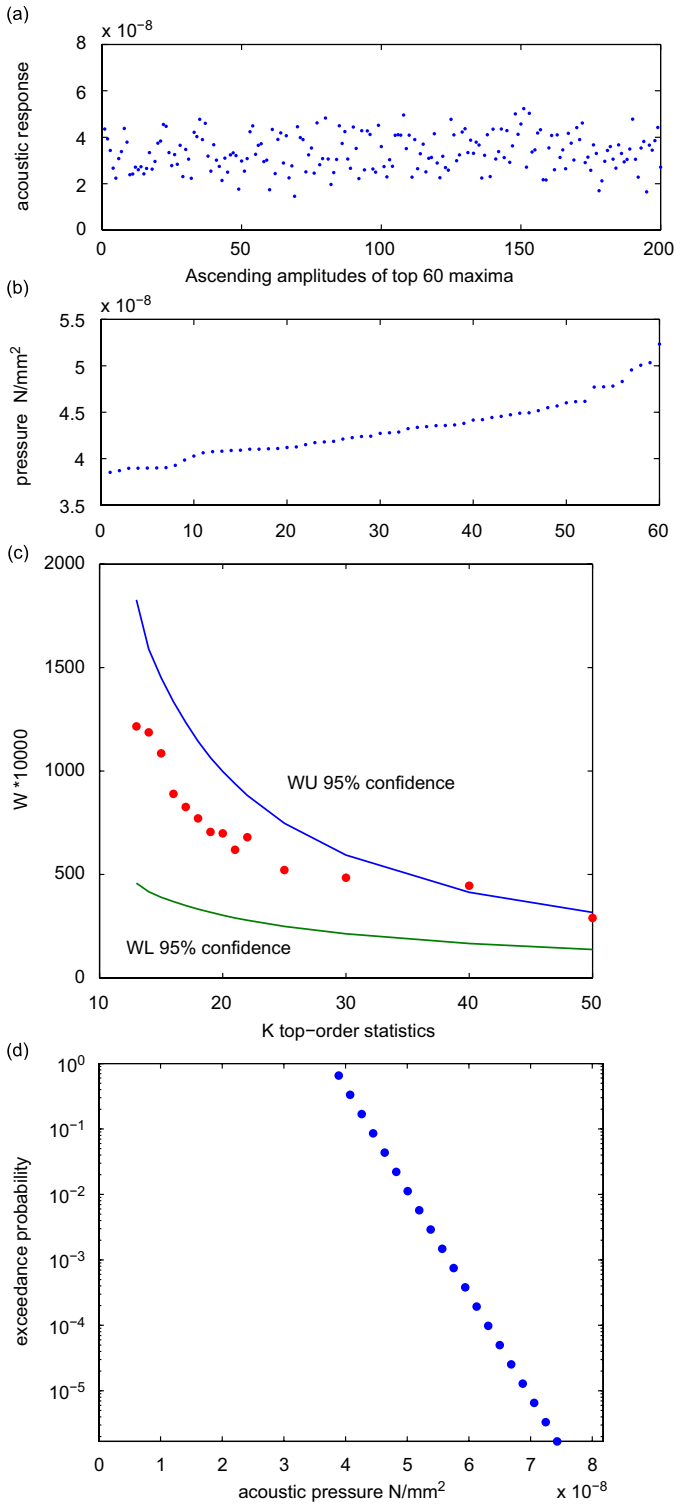

Fig. 26. (a) Top-order statistics; (b) ascending top-order statistics; (c) Hasofer–Wang test; and (d) quantile estimate for acoustic dof 9 001 032 at 87 Hz (normal: CoV = 0.05).

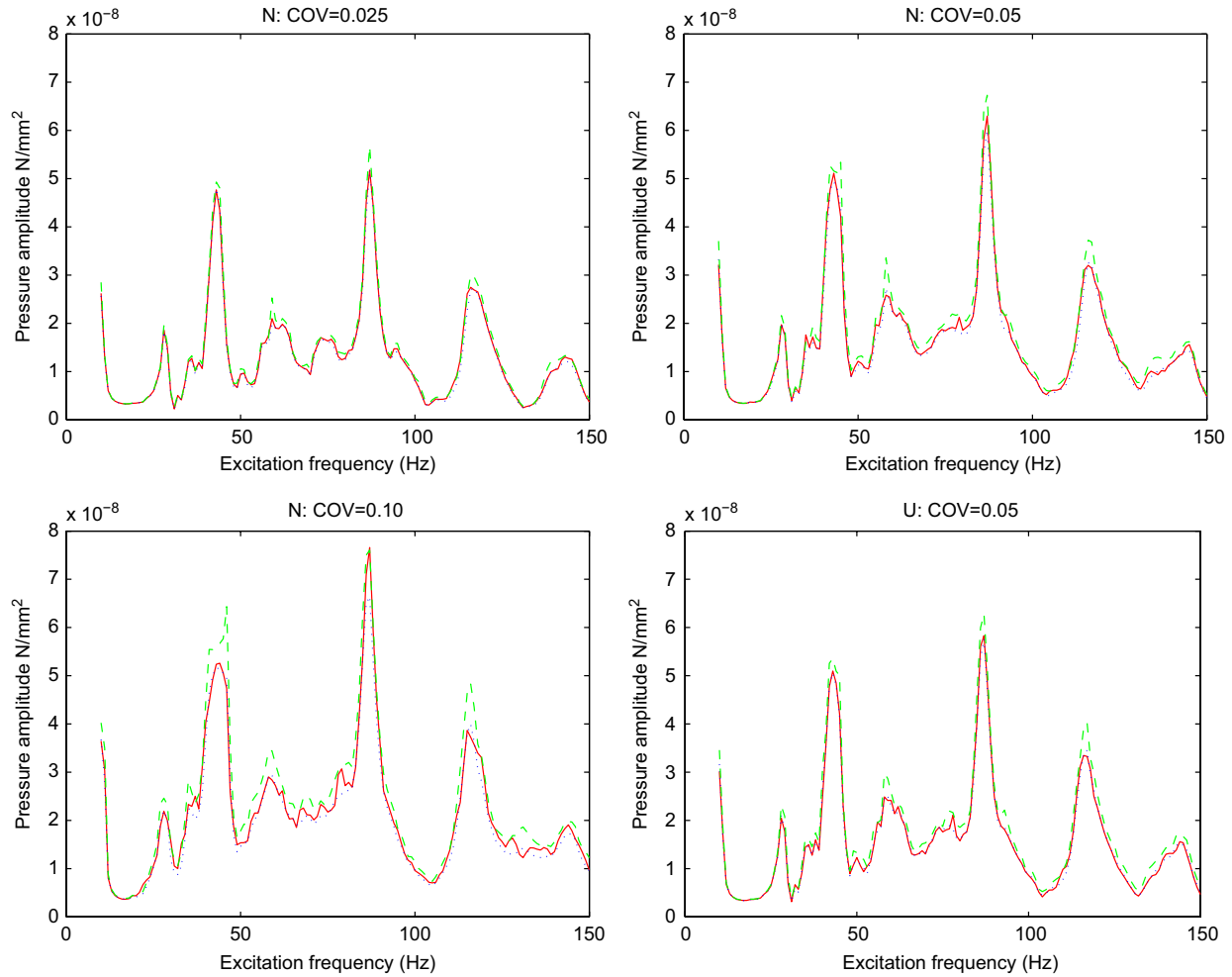

Fig. 27. FRF via quantile estimate ($N_s = 2000$) $p = 0.001$ and 0.0001 Acoustic dof 9001032. Maximum for 2000 runs: ——; prob = 0.001: ·····; and prob = 0.0001: – – –.

Fig. 24 shows for each level of variability the maximum, minimum, and mean acoustic FRF at a 'driver ear' position within the box (air model grid 1001032). Fig. 25 shows for each level of variability, histograms for the number of modes (roots) below 350 Hz derived from the 2000 NASTRAN calculations. This shows a number of things: (i) that uncertainty in the model parameters causes large deviations from the nominal FRF amplitudes and that the variability in the response increases nonlinearly with the level of uncertainty in the input parameters; (ii) the mean response becomes smooth, that it can differ markedly from the nominal response, and is of little practical value; (iii) the response statistics for Gaussian and Uniform distributions, with the same levels of variability, are practically identical; and (iv) the distribution of the mode count appears to be normal below 350 Hz, but the central value of mode count below 350 Hz, increases with COV (an unexpected result).

Turning to the application of the EV theory of chapter 2 for bounding both the structural and acoustic FRFs for this model, Fig. 26 shows information relating to acoustic Grid 90010132 (at 'driver ear' position), at 87 Hz for the normal distribution COV = 0.05 case. Fig. 26a shows for example, 200 randomly selected samples from the 2000 samples available. Fig. 26b also shows 60 top-order statistics (in ascending order). Fig. 26c shows the Hasofer–Wang test Eq. (23), applied to the randomly selected 200 data samples top-order statistics in the region $k = 1.5\sqrt{n}$. Fig. 26d shows, using the entire 2000 samples available, the Type I quantile

estimate based on the *m-observational return level* for exceedance probability $= 1/m$ using Eq. (20). Fig. 27 shows for acoustic dof Grid 9001032, quantile-based FRF bounds (fitted using the entire sample $N_s = 2000$ points) at two exceedance probability levels, namely $p = 1/m = 10^{-3}$ and $p = 1/m = 10^{-4}$. These bounds are predicted across the frequency range at the four levels of variability, and compared in each case with the maximum response levels obtained directly using the entire sample of 2000 points. If it is assumed that the maximum of the 2000 points is prone to very little scatter, predicted bounds corresponding to $p = 1/m = 10^{-3}$ using all 2000 data points to fit the model, as shown in Fig. 27, still appear conservative (whereas a consistent unbiased prediction would have been based on $p = 1/m = 1/2000 = 0.5 \times 10^{-3}$). Since it was shown in Section 3 that predicted bounds will have a small conservative bias, choosing $p = 10^{-3}$ in this case offers an empirical way of compensating for the observed bias, i.e. a form of calibration. Fig. 28 uses this calibration to show the sound pressure FRF at all four parameter variability levels also for acoustic dof Grid 9001032. These FRFs are shown across the entire frequency range using the Weissman estimator at $p = 1/m = 10^{-3}$. Three values of sample size N_s are used with data randomly selected from the 2000 samples available. The sample sizes are $N_s = 500$, 200 and 100 as shown. Again, the top-order statistic $k = 1.5\sqrt{N_s}$ is used in all of the estimates. Figs. 29–31 show similar information to Fig. 28 but for the acceleration FRF in three directions of one particular location.

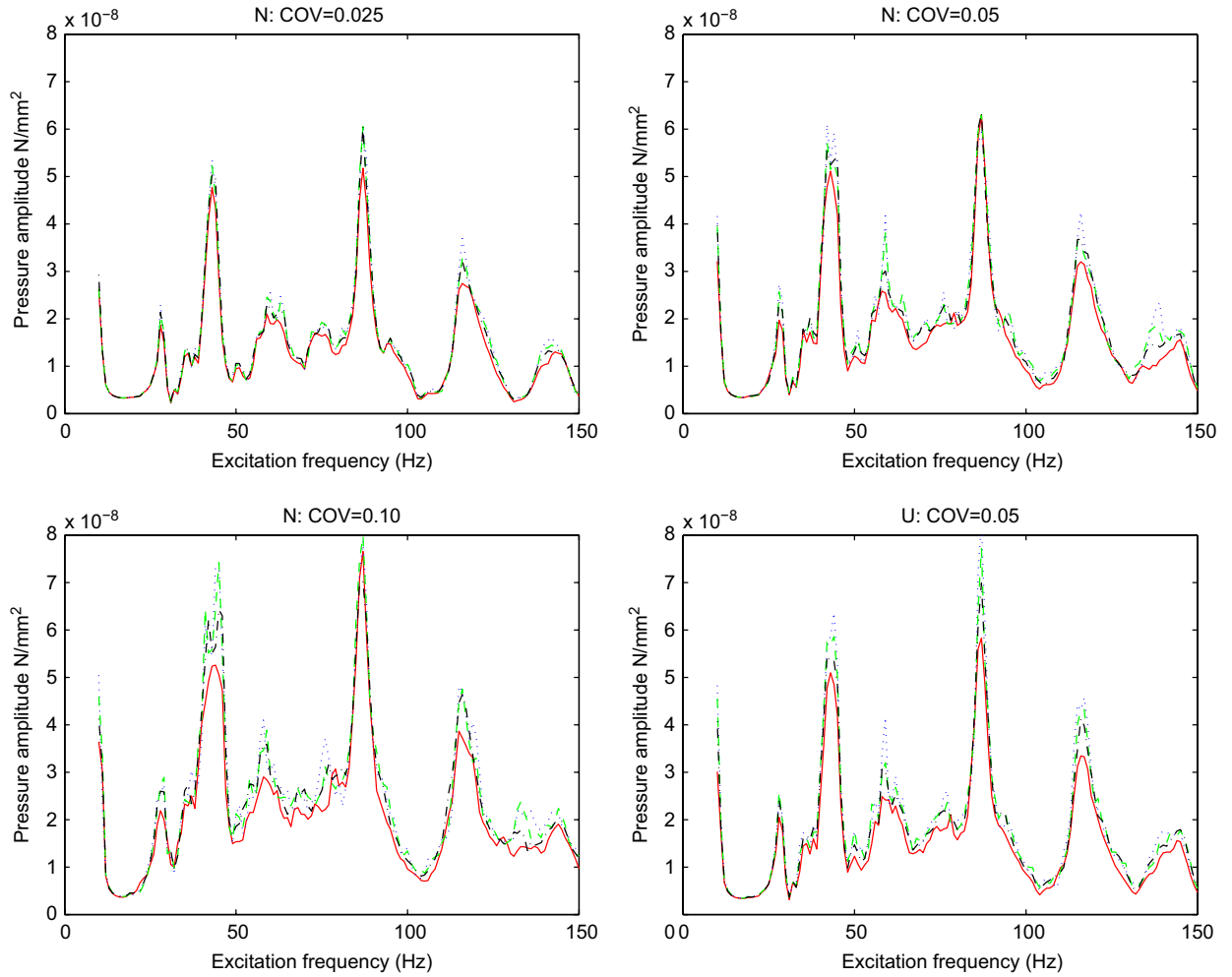

Fig. 28. FRF via quantile estimate ($p = 0.001$) for $N_s = 100$, 200, 500: acoustic dof 9001032. Maximum for 2000 runs: ——; $N_s = 100$: ·····; $N_s = 200$: – – –; and $N_s = 500$: – · – .

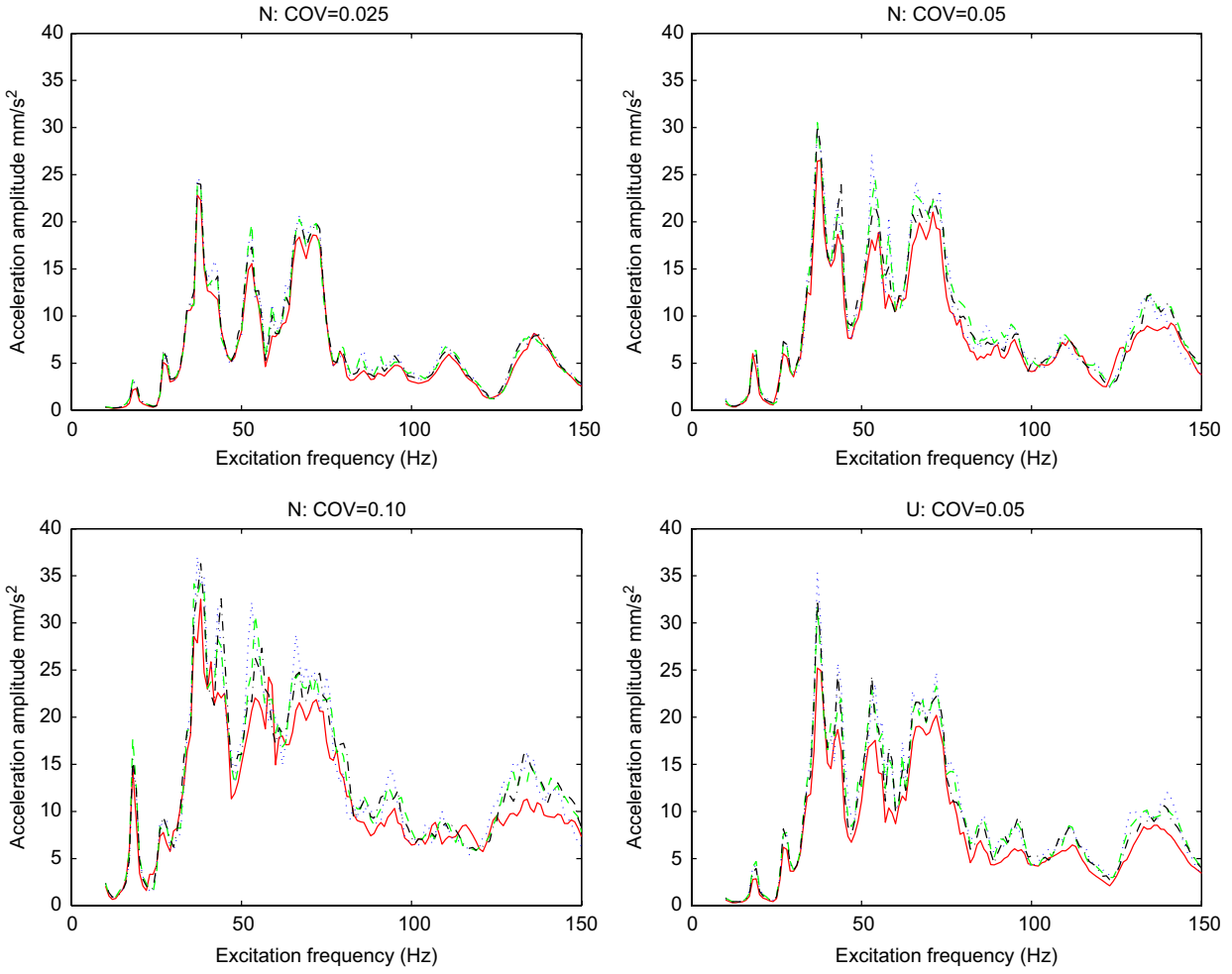

Fig. 29. FRF via quantile estimate ($p = 0.001$) for $N_s = 100$, 200, 500: dof G14610-X. Maximum for 2000 runs: ——; $N_s = 100$: ·····; $N_s = 200$: – – –; and $N_s = 500$: – · – .

5.1. Discussion of results for the box model

The Hasofer–Wang hypothesis test result in Fig. 26b confirms that extreme responses of the box structure do indeed belongs to a Type I domain of attraction. This justifies the use of Eq. (20), namely a Weissman estimator Type I. Numerous other Hasofer–Wang tests (not shown) using data corresponding to different locations on the box, all point to Type I EVs. A response prediction using the Weissman estimator (at a particular exceedance probability level p) can be construed as the level that would be exceeded, on average, once every $m = 1/p$ structures. Fig. 27 shows using all 2000 data points to predict bounds for the exceedance probability levels $p = 10^{-3}$ and 10^{-4}, that even the smaller value $m = 1/p = 1000$ conservatively bounds the maximum values for the 2000 NASTRAN runs. Good results would be expected here since the Weissman estimates use all 2000 data points (a number that would not normally be available). By fixing at this 'calibration' $p = 1/m = 10^{-3}$, Figs. 28–31 show the effect when the size of the random sub-sample N_s is varied. It is noted from Figs. 28–31 that for low parameter variability levels, the predicted FRFs are not sensitive to N_s. At higher levels of CoV there is some influence, but predictions do indeed bound the maximum FRF based on the full data sample. In the NVH context, this would provide the design engineer with precisely the information needed to decide whether a particular structure, with known parameter variability levels, is acceptable.

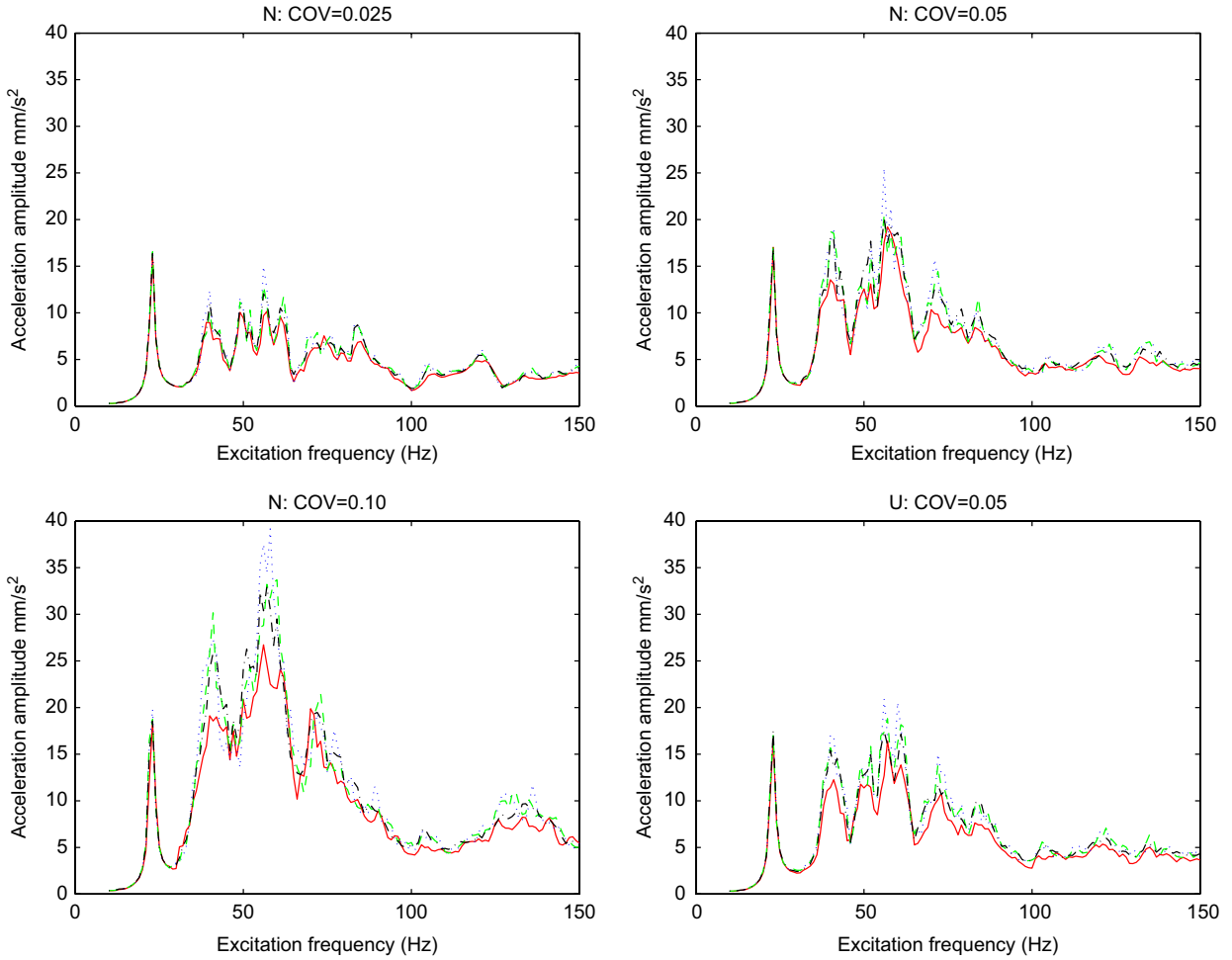

Fig. 30. FRF via quantile estimate ($p = 0.001$) for $N_s = 100$, 200, 500: dof G14610-Y. Maximum for 2000 runs: ——; $N_s = 100$: ·····; $N_s = 200$: – – –; and $N_s = 500$: — · — .

6. Conclusions

An FRF bounding method has been tested using small amounts of simulated data to make predictions that relate to the probabilistic responses of a substantially larger batch of uncertain structures. This bound is based on repeatedly fitting a Weissman predictor namely an optimally inverted Type I asymptotic threshold exceedance model at discrete frequencies. This is used to predict the '*m*-observational return level', i.e. the level that will be exceeded on average once in every *m* structures realised. Confirmation that the data is indeed Type I is justified at each frequency by use of the dedicated Hasofer–Wang hypothesis test. The method has been tested on several types of uncertain linear structure, initially on both sdof and appropriately sized mdof systems to establish its scope and limitations, and then on two structures coupled to an acoustic cavity, namely a fully random grillage, and a partially random industrial-scale box structure. First regarding the scope and limitations of the method, the evidence points to the following conclusions:

- For an (uncoupled) sdof system, and for very small uncoupled mdof structures, both with appropriately random mass and stiffness but deterministic damping, the method should not be used at resonant frequencies because extreme responses are physically bounded, i.e. independent of the mass and stiffness, and are not of Type I. Away from resonance, the method can be used because responses appear to be Type I.

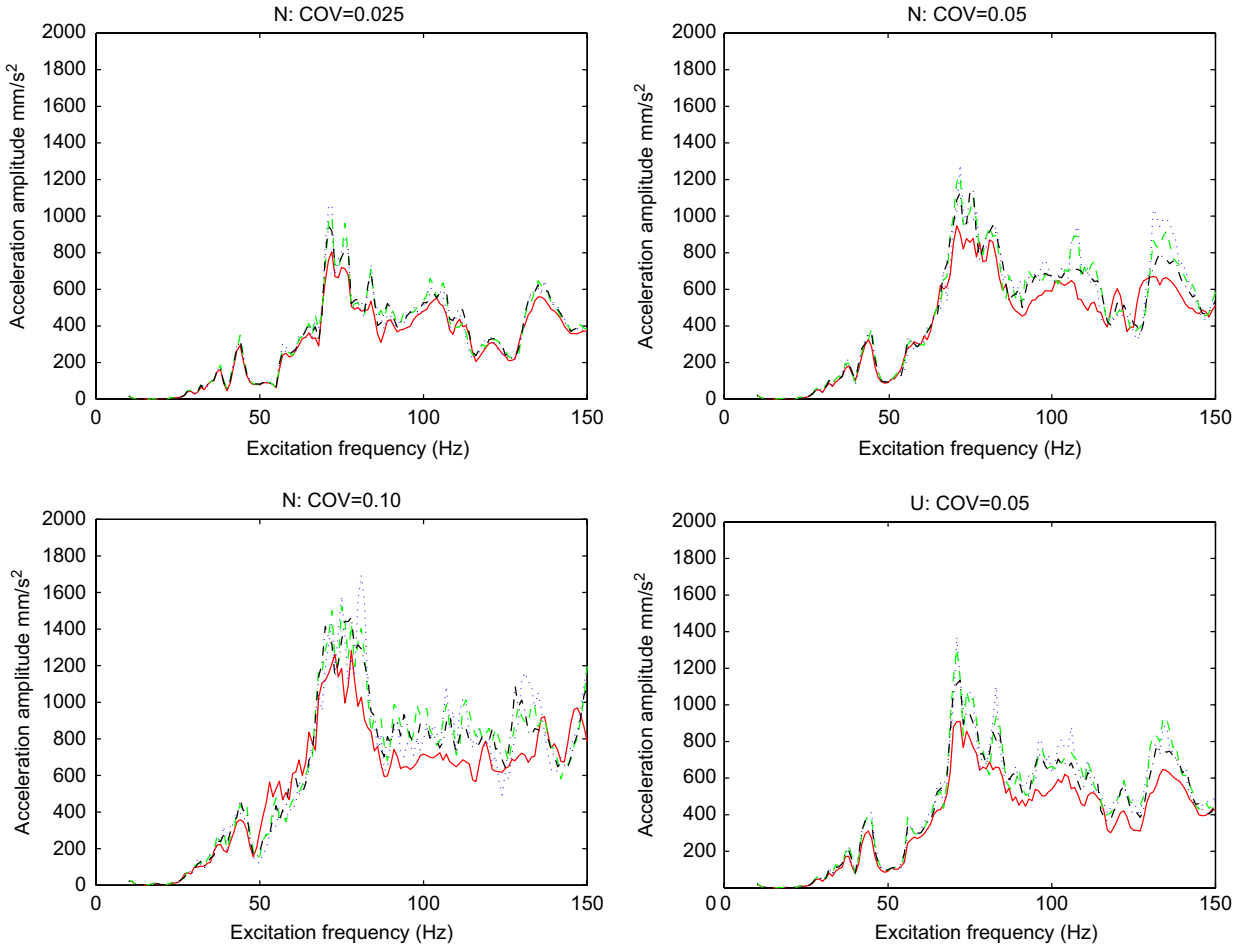

Fig. 31. FRF via quantile estimate ($p = 0.001$) for $N_s = 100$, 200, 500: dof G14610-Z. Maximum for 2000 runs: ——; $N_s = 100$: ·····; $N_s = 200$: – – –; and $N_s = 500$: – · – .

For larger mdof systems, still with deterministic damping, the method can be used even at resonant frequencies (if justified by the Hasofer–Wang test) because responses appear to rapidly become Type I.

- For uncoupled sdof and very small uncoupled mdof structures, with random mass, stiffness, and normally distributed damping, the method can be used because responses appear to be Type I. But for uniformly distributed damping, responses of small mdof systems may not be Type I and therefore the method should not be used.
- If the response of an uncoupled structure at a low frequency resonant peak is shown to be Type I, a similar low frequency resonant response of the same structure when coupled to an acoustic cavity is even more likely to be Type I owing to the participation of the acoustic modes which is expected to provide additional randomisation of a resonant peak.
- If the response of either an uncoupled or coupled structure at a low frequency resonant peak is shown to be Type I, it is even more likely to be Type I at higher frequencies owing to the increased participation of both structural and acoustic modes.
- The mean value of predicted FRF bounds is moderately conservative, with a small consistent bias above the true m-observational return level.

Regarding application to both types of structure coupled to an acoustic cavity, at all low frequency resonant peaks examined, all responses are shown to be Type I confirming that prediction of probabilistic bounds is

wholly justified. For the fully random grillage structure, the predicted bounds appear to be consistent and accurate. With regard to the industrial-scale box structure using the necessarily restricted data available, the evidence would also suggest that the predicted bounds are moderately conservative. It is also shown that less conservative bounds can easily be calibrated to give very acceptable FRF bounds for engineering purposes.

References

[1] C. Soize, Random matrix theory and on non-parametric random uncertainties in vibration analysis, *Journal of Sound and Vibration* 263 (2003) 893–916.

[2] B. Mace, P. Shorter, A local modal perturbation method for estimating frequency response statistics of built-up structures with uncertain properties, *Journal of Sound and Vibration* 242 (2001) 793–811.

[3] B. Mace, Preface—uncertainty in dynamics, *Journal of Sound and Vibration* 288 (2005) 423–429.

[4] P. Shorter, R. Langley, Vibro-acoustic analysis of complex systems, *Journal of Sound and Vibration* 288 (2005) 669–699.

[5] A. Keane, W. Price (Eds.), *Statistical Energy Analysis*, Cambridge University Press, Cambridge, 1997.

[6] B. Mace, The statistical energy hypothesis of coupling power proportionality and some implications of its failure, *Journal of Sound and Vibration* 178 (1994) 95–112.

[7] V. Cotoni, R. Langley, M. Kidner, Numerical and experimental validation of variance prediction in the statistical energy analysis of built-up systems, *Journal of Sound and Vibration* 288 (2005) 701–728.

[8] R. Langley, The dynamic analysis of uncertain structures (Plenary Paper), *The Seventh International Conference on Recent Advances in Structural Dynamics*, ISVR, Southampton, 2000.

[9] R. Melchers, *Structural Reliability and Prediction*, second ed., Wiley, New York, 1999.

[10] M. Hohenbichler, R. Rackwitz, Improvement of second-order reliability estimates by importance sampling, *Journal of Engineering Mechanics* 114 (1988) 2195–2199.

[11] M. Evans, T. Swartz, *Approximating Integrals via Monte-Carlo and Deterministic Methods*, Oxford University Press, Oxford, 2000.

[12] K. Breitung, Probability approximations by log likelihood maximization, *Journal of Engineering Mechanics, American Society of Civil Engineers* 117 (1991) 457–477.

[13] K. Breitung, L. Faravelli, Response surface methods and asymptotic approximations, *Mathematical Models for Structural Reliability Analysis*, CRC Press, Boca Raton, 1996.

[14] D. Johnson, Probabilistic and Possibilistic Models for Uncertainty for Static and Dynamic Structures, PhD Dissertation, University of Cambridge, 2001.

[15] A. Der Kiureghian, J. Ke, The stochastic finite element method in structural reliability, *Probabilistic Engineering Mechanics* 3 (1988) 83–91.

[16] I. Elishakoff, Y. Ren, The bird's eye view on finite element method for structures with large stochastic variations, *Computer Methods in Applied Mechanics and Engineering* 168 (1999) 51–61.

[17] O. Dessombz, F. Thouverez, J.P. Laine, L. Jezequel, Analysis of mechanical systems using interval computations applied to finite element methods, *Journal of Sound and Vibration* 239 (2001) 949–968.

[18] S. Rao, L. Berke, Analysis of uncertain structures in structural systems using interval analysis, *AIAA Journal* 35 (1997) 727–735.

[19] S. Nakagiri, K. Suzuki, Interval estimation of eigenvalue value problem based on finite element sensitivity analysis and convex model, *Transactions of Japanese Society of Engineers, Series A* 40 (1997) 228–233.

[20] C. Pantelides, S. Ganzerli, Design of trusses under uncertain loads using convex models, *Journal of Structural Engineering, ASCE* 124 (1998) 318–329.

[21] M. Hanss, The transformation method for the simulation and analysis of systems with uncertain parameters, *Fuzzy Sets and Systems* 130 (3) (2002) 277–289.

[22] S. Donders, D. Vandepitte, J. Van de Peer, W. Desmet, Assessment of uncertainty on structural dynamic responses with the short transformation method, *Journal of Sound and Vibration* 288 (2005) 523–549.

[23] Q. Zhiping, G. Yuanxian, Interval parameter perturbation method for evaluating the bounds on natural frequencies of structures with interval parameters, *Acta Mechanica Solida Sinica (English series)* 11 (1998) 56–62.

[24] D. Moens, D. Vandepitte, A fuzzy finite element procedure for the calculation of uncertain frequency response functions of damped structures: part 1—procedure, *Journal of Sound and Vibration* 288 (2005) 431–462.

[25] H. De Gersem, D. Moens, W. Desmet, D. Vandepitte, A fuzzy finite element procedure for the calculation of uncertain frequency response functions of damped structures: part 2—numerical case studies, *Journal of Sound and Vibration* 288 (2005) 463–486.

[26] G. Manson, Calculating frequency response for uncertain systems using complex affine analysis, *Journal of Sound and Vibration* 288 (2005) 487–521.

[27] O. Gianni, M. Hanss, Model reduction for uncertainty quantification of mechanical structures by component mode synthesis method, *The Ninth International Conference on Recent Advances in Structural Dynamics*, Southampton, 2006.

[28] L. Hinke, B. Mace, T. Waters, Modelling uncertainty using nondeterministic modal superposition, *The Ninth International Conference on Recent Advances in Structural Dynamics*, Southampton, 2006.

[29] S. McWilliam, Frequency response function analysis of uncertain structures: the vertex identification method, *The Ninth International Conference on Recent Advances in Structural Dynamics*, Southampton, 2006.

[30] S. Coles, *An Introduction to Statistical Modelling of Extreme-Values*, Springer, London, 2001.

[31] E. Castillo, A. Hadi, N. Balakrishnan, J. Sarabia, *Extreme-value and Related Models with Applications in Engineering and Science*, Wiley, New York, 2005.
[32] A. Hasofer, Non-parametric estimation of failure probabilities, in: F. Casciati, J.B. Roberts (Eds.), *Mathematical Models for Structural Reliability Analysis, Mathematical Modelling Series*, CRC Press, Boca Raton, 1996, pp. 195–226 (Chapter 4).
[33] I. Weissman, Estimation of parameters and large quantiles based on the k largest observations, *Journal of the American Statistical Association* 73 (364) (1978) 812–815.
[34] J.F. Dunne, M. Ghanbari, Efficient extreme-value predictions for nonlinear beam vibrations using measured random response histories, *Nonlinear Dynamics* 24 (2001) 71–101.
[35] D.E. Newland, *Mechanical Vibration Analysis and Computation*, Longman Scientific & Technical, UK, 1994.
[36] M. Chargin, M.O. Gartmeier, A finite element procedure for calculating fluid structure interaction using MSC NASTRAN, NASA Technical Memorandum 102857, 1990.
[37] L. Kinsler, A. Frey, A. Coppens, J. Sanders, *Fundamentals of Acoustics*, Wiley, New York, 1982.
[38] O. Zienkiewicz, *The Finite Element Method*, McGraw-Hill, New York, 1977, p. 169.
[39] Y. Cheung, M. Yeo, *A Practical Introduction to Finite Element Analysis*, Pitman Publishing, London, 1979, pp. 19–20.
[40] L.W. Dunne, J.F. Dunne, Evaluation of model uncertainty in modal acoustic response analysis, ICSV13, Vienna, 2006.
[41] L Komzsik, *The Lanczos Method—Evolution and Application*, SIAM, Philadelphia, PA, 2003.